Bioorganic Chemistry 146 (2024) 107324

Contents lists available at ScienceDirect

Bioorganic Chemistry

journal homepage: www.elsevier.com/locate/bioorg

Discovery of novel quinolin-2-one derivatives as potential GSK-3β inhibitors for treatment of Alzheimer's disease: Pharmacophore-based design, preliminary SAR, *in vitro* and *in vivo* biological evaluation

Esraa Abdo Moustafa [a], Heba Abdelrasheed Allam [b], Marwa A. Fouad [b,c], Ahmed M. El Kerdawy [b,d], Nahed Nasser Eid El-Sayed [a], Christoph Wagner [e], Hatem A. Abdel-Aziz [f], Manal Abdel Fattah Ezzat [b,*]

[a] Egyptian Drug Authority (EDA), 51 Wezaret El-Zeraa St., Giza 35521, Egypt
[b] Department of Pharmaceutical Chemistry, Faculty of Pharmacy, Cairo University, Kasr El-Aini Street, 11562 Cairo, Egypt
[c] Pharmaceutical Chemistry Department, School of Pharmacy, Newgiza University, Newgiza, km 22 Cairo– Alexandria Desert Road, Cairo, Egypt
[d] School of Pharmacy, College of Health and Science, University of Lincoln, Joseph Banks Laboratories, Green Lane, Lincoln, United Kingdom
[e] Institut für Chemie, Naturwissenschaftliche FakultätII, Universität Halle, Kurt-Mothes-Str. 206120, Halle, Germany
[f] Department of Applied Organic Chemistry, National Research Center, Dokki, Giza, P.O. Box 12622, Egypt

ARTICLE INFO

Keywords:
Alzheimer's disease
Glycogen synthase kinase inhibitor
Quinolin-2-one
Tau hyperphosphorylation, ADME

ABSTRACT

Recently, glycogen synthase kinase-3β (GSK-3β) has been considered as a critical factor implicated in Alzheimer's disease (AD). In a previous work, a 3D pharmacophore model for GSK-3β inhibitors was created and the results suggested that derivative ZINC67773573, **VIII**, may provide a promising lead for developing novel GSK-3β inhibitors for the AD's treatment. Consequently, in this work, novel series of quinolin-2-one derivatives were synthesized and assessed for their GSK-3β inhibitory properties. *In vitro* screening identified three compounds: **7c**, **7e** and **7f** as promising GSK-3β inhibitors. Compounds **7c**, **7e** and **7f** were found to exhibit superior inhibitory effect on GSK-3β with IC_{50} value ranges between 4.68 ± 0.59 to 8.27 ± 0.60 nM compared to that of staurosporine (IC_{50} = 6.12 ± 0.74 nM). Considerably, compounds **7c**, **7e** and **7f** effectively lowered tau hyperphosphorylated aggregates and proving their safety towards the SH-SY5Y and THLE2 normal cell lines. The most promising compound **7c** alleviated cognitive impairments in the scopolamine-induced model in mice. Compound **7c**'s activity profile, while not highly selective, may provide a starting point and valuable insights into the design of multi-target inhibitors. According to the ADME prediction results, compounds **7c**, **7e** and **7f** followed Lipinski's rule of five and could almost permeate through the BBB. Molecular docking simulations showed that these compounds are well accommodated in the ATP binding site interacting by its quinoline-2-one ring through hydrogen bonding with the key amino acids Asp133 and Val135 at the hinge region. The findings of this study suggested that these new compounds may have potential as anti-AD drugs targeting GSK-3β.

1. Introduction

Alzheimer's disease (AD) is an aging-related complex chronic neurodegenerative disorder whose mysterious pathophysiology is not fully understood [1]. Around 50 million patients worldwide experience this ailment and, by 2050, it is projected to be more than tripled, placing a significant financial and health burden on both patients and health care systems [2]. Despite its intricacy, numerous hypotheses have been put out to explain its pathophysiology, including the tau protein hypothesis, the cholinergic theory, amyloid-β (Aβ) protein hypothesis and others [3]. Galantamine, donepezil, rivastigmine and memantine are the only FDA approved drugs for AD, however, all of them are primarily used as palliative care and cannot prevent or reverse AD pathology [4]. As a result, the development of disease modifying therapeutics targeting tauopathy or Aβ deposition is an urgent need [5].

Tau is the binding protein responsible for microtubule construction and stabilization in the normal physiological state. The hyperphosphorylation of tau protein makes it incapable of connecting with

* Corresponding author.
E-mail address: Manal.salem@pharma.cu.edu.eg (M. Abdel Fattah Ezzat).

https://doi.org/10.1016/j.bioorg.2024.107324
Received 17 January 2024; Received in revised form 27 March 2024; Accepted 29 March 2024
Available online 30 March 2024

microtubules. Consequently, the dissociated tau protein self-accumulates and clumps in neurons as toxic neurofibrillary tangles (NFTs), resulting in neuronal death [6,7]. This pathogenic process is hypothesized to be triggered by the dysregulation and mutations in the kinases and phosphatases that interact with tau protein [8].

Kinases are essential enzymes for many vital cell processes, and their dysregulation is considered the primary player in initiating numerous human ailments, including immunological and neurological diseases aside from oncologic-related ones [9]. Glycogen synthase kinase-3β (GSK-3β) has been found to be a crucial protein kinase in the hyperphosphorylation and the pathological accumulation of tau protein [10]. Thus, GSK-3β has been proposed as a promising target for neurodegenerative disorders amongst other diseases [11]. According to the "dual pathway" theory, GSK-3β has been proven to strongly promote the excessive production of Aβ and hyperphosphorylation of tau protein, the key AD neuropathological hallmarks [12]. Besides, aberrant GSK-3β activity is coupled with neuroinflammation and oxidative stress [13]. Accordingly, GSK-3β is engaged in almost all AD's pathological pathways (Fig. 1). As a result, recent research has focused on GSK-3β inhibition, as an effective strategy for treating AD [13].

Nowadays, kinase inhibitors account for 25 % of all ongoing drug discovery research in the pharmaceutical sector [14]. However, clinical trials for ATP competitive inhibitors have frequently failed due to the striking similarities of their targeted ATP pockets what increases the risk of off-target toxicities [15,16]. Owing to the therapeutic significance of kinase inhibitors, several approaches were necessary to surmount kinase drug selectivity hurdle and provide more potent targeted treatments [17]. New promising approaches are to target the inactive conformation of kinases and interacts with their unphosphorylated catalytic site (type II inhibitors) or to design kinase inhibitors with the ability to bind outside the catalytic domain/ATP-binding site and regulate kinase activity by an allosteric mechanism (type III allosteric inhibitors) [18]. For instance, tideglusib is an irreversible allosteric non-ATP competitive GSK-3β inhibitor. Nevertheless, tideglusib did not meet the main end goals in AD patients and phase II clinical trials for tideglusib were discontinued as anti-Alzheimer's medication. Till now, none of the investigated GSK-3β inhibitors reached the market, thus there is a tremendous interest in finding appropriate GSK-3β inhibitors for therapeutic application as Anti-Alzheimer's disease agents [19].

Quinolines and quinolones are heterocyclic privileged scaffolds that typically function as structural building blocks for several complex natural products [20]. Furthermore, they demonstrated several biological and pharmacological effects including anti-Alzheimer activity [21]. Clinical trials have shown that the 8-hydroxyquinoline derivatives, clioquinol **I** and PBT2 **II** (Fig. 2), are strong metal chelators that significantly improved cognition by lowering the levels of Aβ in cerebrospinal fluid (CSF) [22,23]. Recent studies have demonstrated that the quinolin-2(1*H*)-one derivatives **III** and **IV** act as multitargeted agents exhibiting ROS scavenging ability besides their strong cholinesterase inhibitory activities [24]. Moreover, 2-heptyl-3-hydroxyquinol-4(1*H*)-one derivative **V** protected neurons from glutamate-induced death in HT22 cells by preventing cellular Ca^{2+} uptake and glutamate-triggered ROS generation [25]. The pyrazolo[3,2-*c*]quinol-4(5*H*)-one derivative **VI** improved Alzheimer's disease-related cognitive impairment through its Phosphodiesterase 9A (PDE9A) inhibitory action [26]. Additionally, the FDA approved quinolin-2(1*H*)-one derivative, brexipiprazole **VII**, is a serotonin-dopamine modulator that controls non-cognitive psychological symptoms associated with Alzheimer's disease dementia [27]. Furthermore, the 2-quinolone derivative ZINC67773573 (**VIII**) (Fig. 2) was computationally identified as a promising lead compound for developing novel GSK-3β inhibitors for AD treatment [28]. ZINC67773573 (**VIII**) displayed a promising predicted binding pattern and binding affinity in molecular docking simulations as it perfectly fitted in the hinge region interacting with the essential amino acids Val135 and Asp133 (Fig. 3). This binding pattern directs the hydrophobic isoindole ring at position 3 towards the hydrophobic side chains of the amino acids Ile62, Val70, Pro136, and Leu188 [28] (Fig. 3).

The natural isatin derivative, indirubin (**IX**) (Fig. 4), is the key ingredient of the traditional Chinese, *Dang Gui Long Hui Wan*, medicinal remedy that is used for chronic myelocytic leukemia (CML) treatment through GSK-3β and CDK2 inhibition [29–32]. Furthermore, indirubin and its derivatives were found to inhibit GSK-3β and further abnormal tau phosphorylation in AD as ATP competitive inhibitors [33]. Indirubins' isatin ring is accommodated in the hinge region of the GSK-3β binding site interacting *via* its carbonyl and NH moieties by hydrogen bonding with the essential amino acids Val135 and Asp133, respectively [32,33].

In light of the previous facts, in the current research, we used the promising hit compound ZINC67773573 (**VIII**) as a starting point for the design of novel series of quinolin-2-one derivatives that preserve the essential pharmacophoric requirements for GSK-3β inhibition (Fig. 4). Three design strategies have been adapted in the current work to boost GSK-3β binding and thereby amplify the inhibitory effect. The first strategy involved the hybridization between the hit compound ZINC67773573 (**VIII**) quinolin-2-one nucleus and indirubin isatin (**IX**) ring to give series (**9a-c**). Furthermore, ring variation of the isatin moiety with 1*H*-pyrrol-2,5-dione **11** and pyrrolidin-2-one **13** was carried out (Fig. 4). Based on the reported importance of the polar region in GSK-3β binding pocket, as fragments accessing and bind to this region enhance potency [34], the second strategy involved replacing the isoindole moiety in the hit compound ZINC67773573 (**VIII**) with a hydrophilic tail extending towards this key polar region giving series (**7a-f**) (Fig. 4). The third strategy involved the structure rigidification of the hit compound ZINC67773573 (**VIII**) through structural fusion of the quinolin-2-one nucleus with the CNS privileged scaffold diazepine heterocycle giving series (**15a-h**) (Fig. 4) [35].

The designed compounds were synthesized and assessed *in vitro* for their GSK-3β inhibitory activity. The mechanism of enzyme inhibition

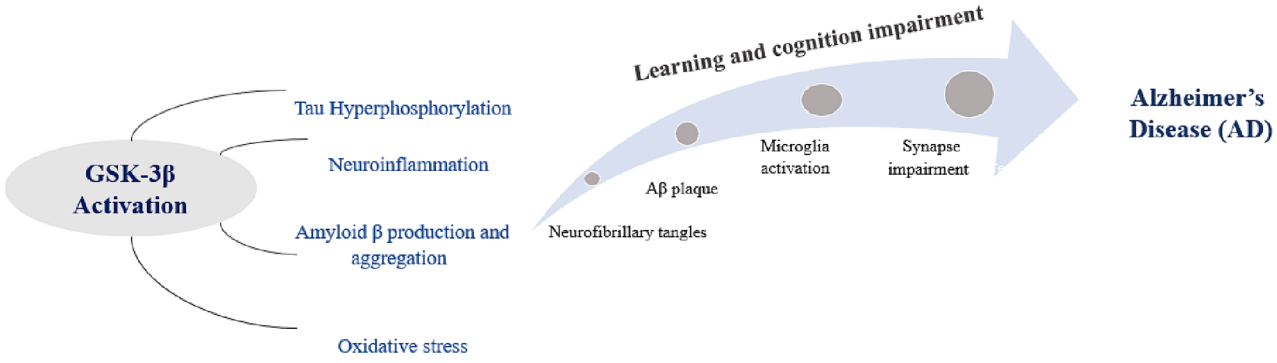

Fig.1. The role of GSK-3β in the development and progression of Alzheimer's disease.

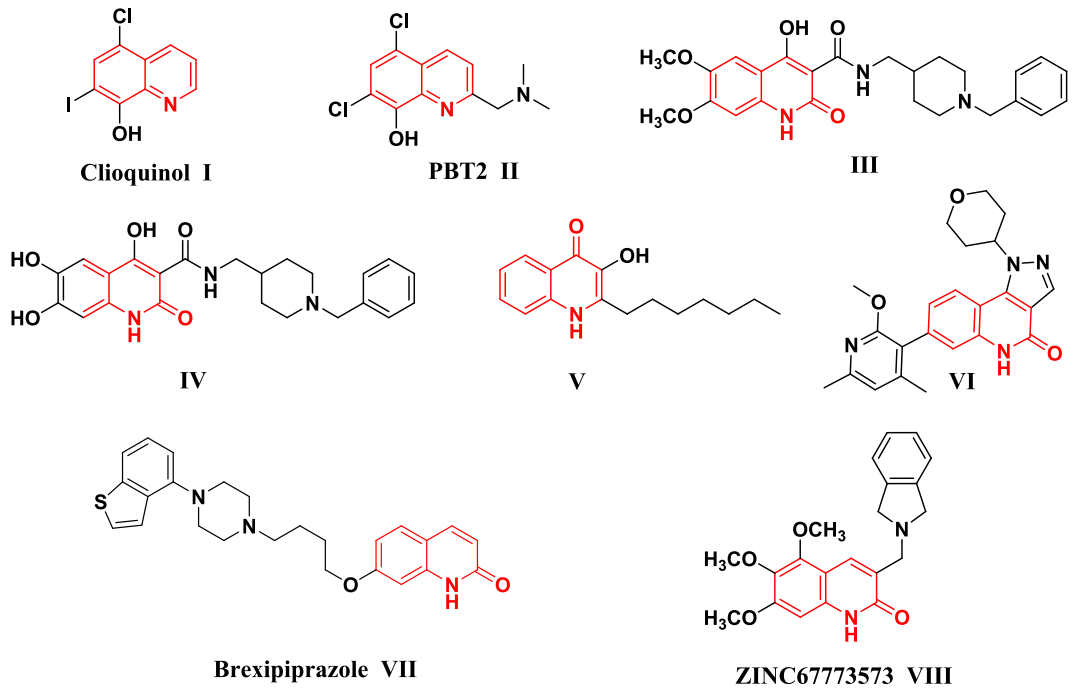

Fig.2. Structures of some anti-Alzheimer's disease compounds with quinoline and quinolone scaffolds.

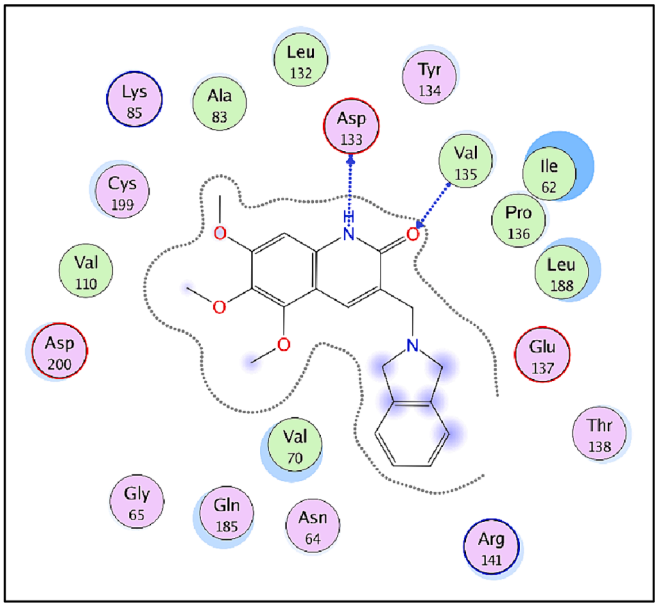

Fig.3. 2D diagrammatic representation of the binding pattern of compound ZINC67773573 (VIII) in GSK-3β kinase domain [28].

for the most potent compound was studied using kinetic analysis. Furthermore, the compound's safety was studied through testing its hepatoma and neuroblastoma cellular toxicity. To test its effect on AD hallmarks, the most potent compounds were tested for their ability to reduce tau hyperphosphorylated aggregates. Finally, *in vivo* neurobehavioral effect of the most potent compound in mice was assessed. Additionally, Molecular docking simulations were performed to inspect the binding pattern of the most potent derivatives with the target kinase, furthermore, *in silico* prediction for BBB permeation and pharmacokinetic properties was carried out.

2. 2-Results and discussion

2.1. Chemistry

A new series of quinolin-2-one derivatives were prepared using 4-hydrazinoquinolin-2(1*H*)-one **5**. Synthesis of the key intermediate **5** was achieved *via* a three-step procedure as outlined in Scheme 1. The first step of the reaction sequence involved one-pot synthesis of 2,4-dichloroquinoline **3** in 92 % yield *via* a cyclocondensation reaction between aniline **1** and malonic acid **2** in the presence of excess of phosphoryl chloride under reflux for 24 h according to the modified procedures described by Mohan [36]. The second step involved regioselective oxidation of 2,4–dichloroquinoline **3** at position-2 *via* treatment with 6 *N* HCl in dioxane [37,38] to produce 4-chloro-2-oxo-quinoline **4** in good yield of 85 %. In the last step, the chloro-product **4** was treated with excess hydrazine hydrate in ethanol [39,40] under reflux for 6 h, thus giving rise to the desired 4-hydrazineylquinolin-2(1*H*)-one **5** in 70 % yield.

Subsequently, the hydrazide **5** was used to synthesize diverse functionalized quinolin-2-one derivatives through reactions with different electrophilic reagents (Schemes 2 & 3). Thus, condensation of hydrazide **5** with the appropriate aromatic aldehydes **6a-f** in absolute ethanol and in the presence of five drops of glacial acetic acid as catalyst produced the corresponding hydrazones 7**a-f** in reasonable yields (>81 %) as single stereoisomers as evidenced by thin layer chromatographic analyses and NMR spectroscopic data. The ^{1}HNMR spectra of these hydrazones lacked the signal due to NH_2 group of the starting material which resonated at $\delta_H = 8.17$ ppm and showed a one proton signal at δ_H values spanning from 8.23 to 8.73 ppm attributable to azomethine proton (CH = *N*-), and two singlet signals at chemical shift values within the range of 10.62–10.82 ppm and of 11.01–11.19 ppm exchangeable with D_2O, attributable to *N*-NH and CO-NH protons, respectively. Moreover, the methoxy groups of derivatives **7a-d** and **7f** appeared at δ_H values within the range of 3.71–3.88 ppm. The ^{13}CNMR spectra indicated the presence of azomethine carbons at δ_C ranging from 144.78 to 148.96 ppm.

Likewise, the reaction of hydrazide **5** with 1*H*-indole-2,3-dione **8a** and its 6-bromo and 6-chloro homologs **8b** and **8c**, respectively, produced the corresponding hydrazones **9a-c** as single products. Thus, the

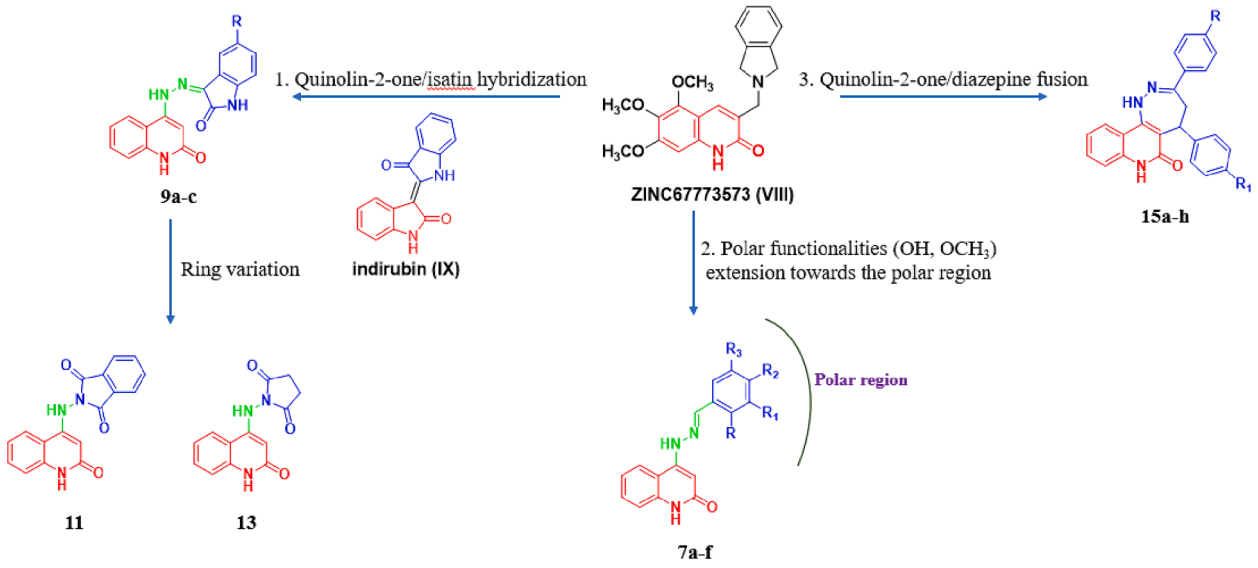

Fig.4. Design strategy of the target novel GSK-3β inhibitors. (Red scaffolds are accommodated in the hinge region).

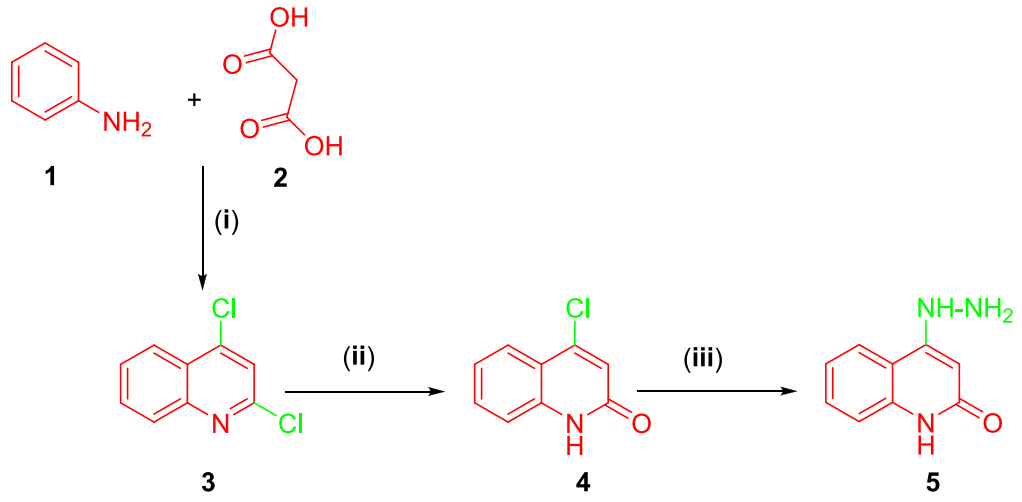

Scheme.1. *Reagents and conditions*: (i) $POCl_3$, reflux 24 h, (ii) 1,4-dioxane, 6 N HCl, reflux 36 h, (iii) 99 % NH_2-NH_2, absolute EtOH, reflux 6 h.

^{1}HNMR spectra indicated the presence of three NH groups resonating at δ_H values within the ranges of 11.35–11.45, 11.45–11.48 and 13.34–13.38 ppm. The ^{13}CNMR spectra showed two amidic carbonyl carbons within the ranges of δ_C = 162.68–162.74 and 163.80–168.5 ppm.

Theoretically, products **7a-f** and **9a-c** may exist as *Z* or *E* stereoisomers or as a mixture of the two isomers depending on the compounds structures and reaction conditions, which can be thermodynamically or kinetically controlled.

Considering compounds **7a-f** the geometry around the (HC = *N*-) bond was assigned as *E*-configuration (Fig. 5) based on the reported data by Wardell and co-workers [41], which indicated that the hydrazones of 4-hydrazinoquinoline adapted an *E* configuration about HC = *N* in their crystal structures with the amine-H atom is directed towards the quinoline residue. In addition to, a previous study [42] supported by X-ray crystallographic analysis showed that the azomethine protons were detected at δ_H values within the range of 7.46–8.80 for *E*-isomers. Furthermore, the CH = hydrazonic carbon atoms were observed at ^{13}C NMR chemical shift values within the range of 139.79–144.78, which are in accordance with the values reported (141.62–148.96 ppm) for similar type of *E*-hydrazones [43] whereas this carbon in *Z*–isomers occurred upfield (δ_C around 136 ppm) [44] Moreover, energy minimization calculations for the two possible geometrical isomers (*E* and *Z*) for these Schiff bases indicated the relative higher stabilities of the *E*-isomers as compared to their *Z*–counterparts (Supplementary Table S5.2), which may suffer from undesirable steric interactions between phenyl proton at *o*-position and NH proton (Fig. 5).

As regard to stereochemical assignment of the C═*N* geometry in derivatives **9a-c**, the following facts and observations have to be considered. First, previous thereortical and experimental studies showed that under thermodynamic conditions (heat treatment), the arylhydrazones of isatin exist most always in the more stablized *Z*-forms, which are capable of forming an intramolecular hydrogen bond [45,46] between hydrazide hydrogen and lactam oxygen of oxoindole ring [N—H—O═C] (Fig. 5), whereas the *E*–isomers, which are formed at 20 °C were considered the less stablesized isomers since they couldn't form such H–bonding interaction. Second, the geometric *Z*–*E* isomerization around C═*N* double bond in isatin hydrazones occurs only *via* a photochemical reaction [47] and the less stabilized *E*-structures slowly thermally isomerized back to the more preferred *Z*–isomers [48].

In this study the products were obtained after heating for 6 h and inspection of their ^{1}HNMR spectra indicated a downfield shift in the chemical shift value of the signal related to the hydrazide-NH proton from 8.17 ppm to higher δ_H values of 13.80, 13.35, 13.34 ppm,

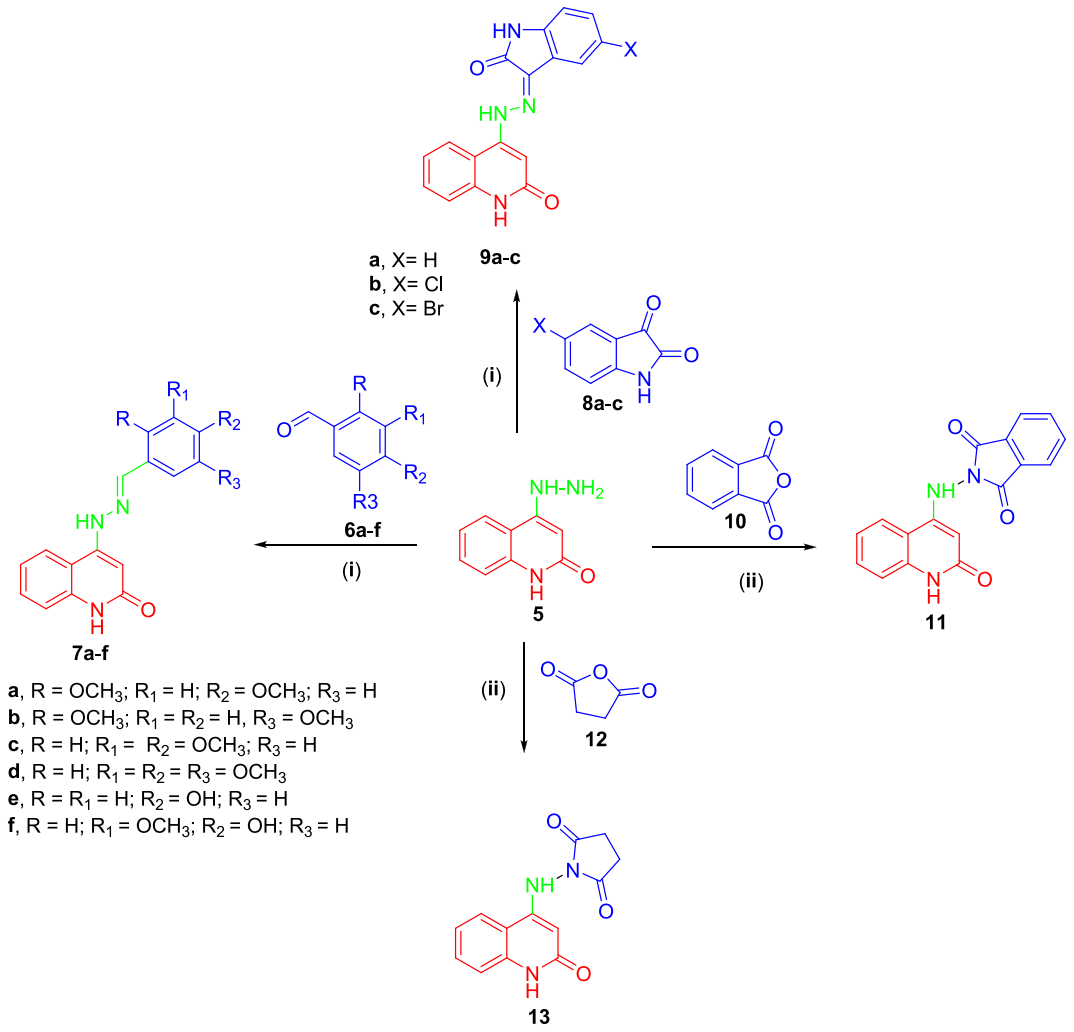

Scheme.2. *Reagents and conditions:* (i) Absolute ethanol, 5 drops of glacial acetic acid, reflux 24–48 h, filtration; (ii) Anhydrous sodium acetate, glacial acetic acid, reflux 24 h.

respectively, indicating a deshielding effect, which could be attributed to its participation in H–bonding intercation with oxoindole's carbonyl group. These recorded ^{1}H NMR shift values are consistent with those reported for a comparable kind of an isatin derived-*Z*-Sciff base (13.95 ppm) [45].

Consequently, products **9a**–**c** were assigned the *Z*-configuration. This assignment is corborated by energy minimization calculations, which indicated the higher energies of *E*-isomers compared to their counterparts *Z*-isomers (Supplementary Table S5.2). The higher energies of *E*-isomers could be attributed to the existence of the destabilizing steric hindrance between 4-H-oxoindole ring and NH-hyrdazide, and this makes it possible to exculde *E*-strcuture from consideration (Fig. 5).

Thereafter, the synthesis of hybrid quinolinone-pyrrolidindione derivatives including 2-[(2-oxo-1,2-dihydroquinolin-4-yl)amino]isoindoline-1,3-dione **11** and 1-[(2-oxo-1,2-dihydroquinolin-4-yl)amino] pyrrolidine-2,5-dione **13** were readily achieved by heating under reflux a mixture of hydrazide **5** with phthalic anhydride **10** or succinic anhydride **12** in acetic acid containing sodium acetate for 24 h. Mechanistically, these reactions involved ring opening *via* nucleophilic attack by the hydrazinyl amino group on one of the carbonyl groups to produce monoamide mono acid intermediates **A** & **B** (Fig. 6), which then underwent intramolecular cyclization thereby furnishing the pyrrolidindione derivatives **11** and **13**, as evident from their ^{1}HNMR spectra, which exhibited only two singlet signals attributable to two NH groups resonating at δ_H values of 9.64 and 11.21 ppm for derivative **11** and at 9.37 and 11.13 for derivative **13**. Furthermore, ^{13}C NMR spectra confirmed the formation of the symmetric pyrrolidine-2,5-dione rings by displaying the characteristic carbon resonances at δ = 166.10 and 174.40 ppm assignable to the two equivalent dione carbons in compounds **11** and **13**, respectively.

Last, the potassium carbonate mediated reaction of hydrazide **5** with various chalcone derivatives **14a-h** in absolute methanol (Scheme 3) afforded 3,5-diaryl-1,4,5,7-tetrahydro-6*H*-[1,2]diazepino[4,3-*c*]quinolin-6-one derivatives **15a-h** instead of the expected pyrazoline derivatives **16a-h** as evident from their spectroscopic data and the X-ray crystallographic analysis of derivative **15c** (Fig. 7 and Supplementary Tables S5.3). The exclusion of pyrazoline derivatives was based on the presence of two NH signals resonating within the chemical shift ranges of 10.17–10.37 and 11.22–11.30 ppm. Furthermore, the ^{1}HNMR spectra of compounds **15a-h** lacked the signal due to olefinic proton at chemical shift of 5.72 ppm of the starting hydrazide **5** and they indicated the nonequivalence of the two geminal protons (H_A & H_B) at C^4 in the diazepine ring due to the creation of a new stereogenic center at C^5 of diazepine ring. Thus, one of these diastereotopic protons (H_A) at δ_H = 3.60–3.65 ppm exhibited a typical ABX spin system with the characteristic multiplicity pattern of doublet of doublet due to geminal coupling with H_B (at δ_H = 3.03–3.10 ppm) with coupling constant $^{2}J_{AB}$ values within the range of 13.7—14.2 Hz and the vicinal coupling with H_X (at δ_H = 5.06—5.15 ppm) with coupling constant $^{3}J_{AX}$ values within the range of 5.8–6.1 Hz for compounds **15a-d**, while for derivatives **15e-**

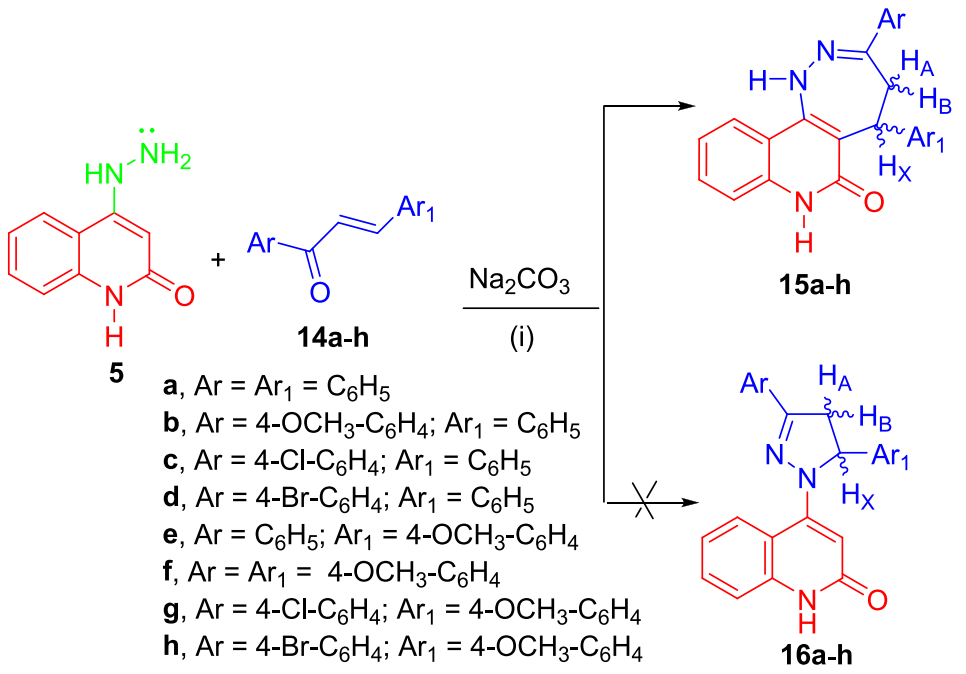

Scheme.3. *Reagents and conditions*: (i) Absolute methanol, anhydrous K_2CO_3, reflux 30–48 h.

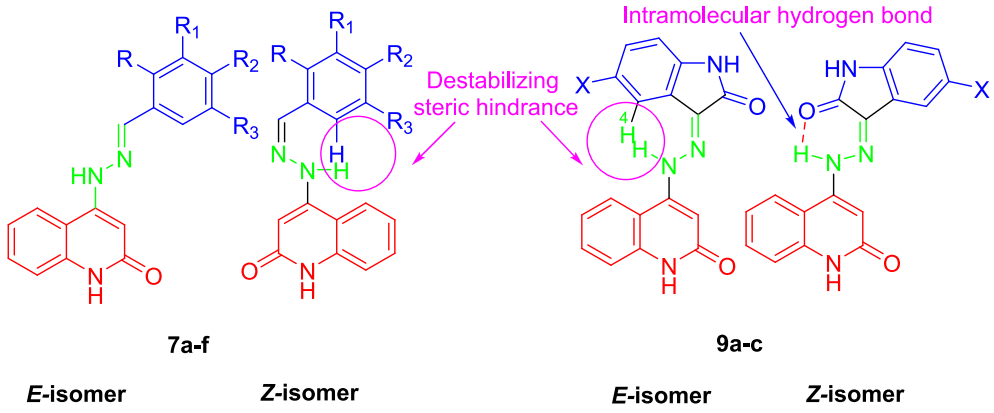

Fig.5. E and Z isomers of hydrazones **7a-f** and **9a-c**. The steric hindrance in the *Z*-isomers of derivatives **7a-f** and *E*-isomers of **9a-c** as well as stabilizing intramolecular hydrogen bonding interactions in *Z*-isomers of compounds **9a-c**.

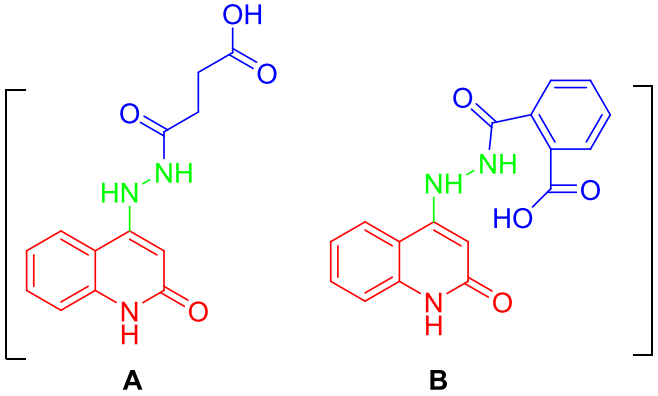

Fig.6. The expected opened intermediates in the reaction of hydrazide **5** with acid anhydrides.

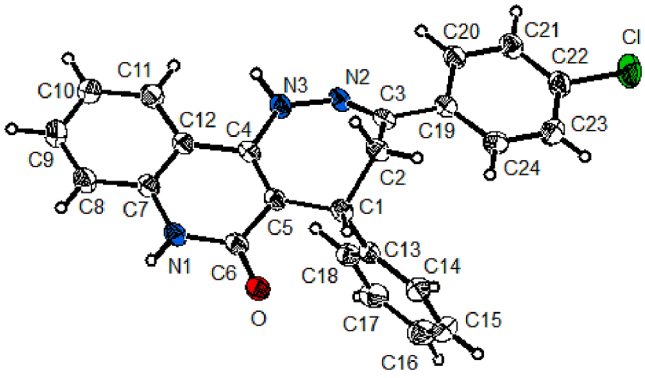

Fig.7. Molecular structure of 3-(4-chlorophenyl)-5-phenyl-4,5-dihydro-1H-[1,2]diazepino[4,3-*c*]quinolin-6(7H)-one 15c in the crystal. Thermal ellipsoids are shown at 50 % probability level.

h, the signal due to H_A is overlapped with the methoxy signals. However, the second diastereotopic proton (H_B) showed only the geminal coupling (^2J 12.5–14.0 Hz). Moreover, the ^{13}CNMR spectra showed the methylene and the methine groups at δ_C ranges of 41.84–42.91 and 37.91–38.32 ppm in order.

The plausible mechanism for the formation of diazepine derivatives **15a-h** is depicted in Fig. 8. This mechanism could be rationalized in terms of chemical reactivity of 4-hydrazineylquinolin-2(1*H*)-one **5**, in which the third position in the 2(1*H*)-quinolone ring is highly activated, because of the influence of the hydrazinyl group with electron-donating properties and the electron-withdrawing effects of the carbonyl oxygen atom at the position-2. Therefore, the mechanism started by tautomerization of compound **5** to its tautomeric form **5′**, followed by proton loss to produce the stabilized anionic species **A** [49]. Due to the Michael acceptor activity of the α, β-unsaturated carbonyl system under basic catalysis [50], the Π-nucleophilic carbon C^3 attacked the electron-deficient-β-carbon of the chalcone molecule, thereby generating the enolate **B**. A proton transfer to **B** released the less stable enol form **C**, which in turn underwent tautomerization to liberate the Michael addition adduct **D**. Ring closure took place *via* intramolecular nucleophilic attack by the primary nitrogen onto the carbonyl group through 7–*endo*–*trig*-cyclization to give the cyclized structure **E**, which upon losing a water molecule produced diazaepino compounds having structure **F**, which tautomerized to the final products **15a-h**. Thus, this regioselective cyclization reaction between 4-hydrazineylquinolin-2(1*H*)-one or its derivatives with various chalcones can be considered an interesting route for the synthesis of the novel class of [1,2]diazepino[4,3-*c*]quinoline-6-one derivatives similar to **15a-h**.

Spectroscopic data and X- ray characterization of compound 15c.

The reaction of 4-hydrazinylquinolone with 4-chlorochalcone in refluxing MeOH and in the presence of anhydrous potassium carbonate, afforded a single product **15c**. The ^{1}H NMR spectrum exhibited two D_2O exchangeable signals of 2NH groups at chemical shift values δ_H 10.36 and 11.28 ppm in addition to three signals of ABX system around δ_H 3.08, 3.65 and 5.15 ppm. The two sp^3 carbons of the latter system appeared near δ_c 37.97 and 42.77 ppm in its ^{13}C NMR spectrum due to methylene CH_AH_B and methine CH_X, respectively. These spectroscopic data of the reaction product and its satisfactory H, C, N elemental analysis supported the diazepine structure **15c** rather than the pyrazoline structure **16c** as postulated in Scheme 3. Undoubtedly, X-ray diffraction of **15c** (Fig. 7) confirmed the construction of the diazepine ring and ruled out the formation of its structural isomeric pyrazoline ring. Characteristic bond lengths of diazepine **15c** and the torsion angles of its essential bonds are listed in Supplementary Tables S5.3.

2.2. Biological assay

2.2.1. In vitro GSK-3β inhibition and SAR evaluation

Using pan-kinase inhibitor, staurosporine, as a reference standard, the synthesized compounds' ability to inhibit GSK-3β was assessed applying ATP-Glo assay technique [51]. As depicted in Table 1, except for compounds **9b** and **15 g**, most compounds had outstanding inhibitory behavior at the nanomolar level. Compounds **7c**, **7e**, **7f**, **15a** and **15d** demonstrated excellent inhibitory performance (IC_{50} ranging between 4.68 ± 0.59 to 10.92 ± 0.74 nM) compared with the reference drug staurosporine (IC_{50} = 6.12 ± 0.74 nM). Compound **7c,** in particular, was found to exhibit superior inhibitory effect on GSK-3β with IC_{50} value of 4.68 ± 0.59 nM compared to that of staurosporine (IC_{50} = 6.12

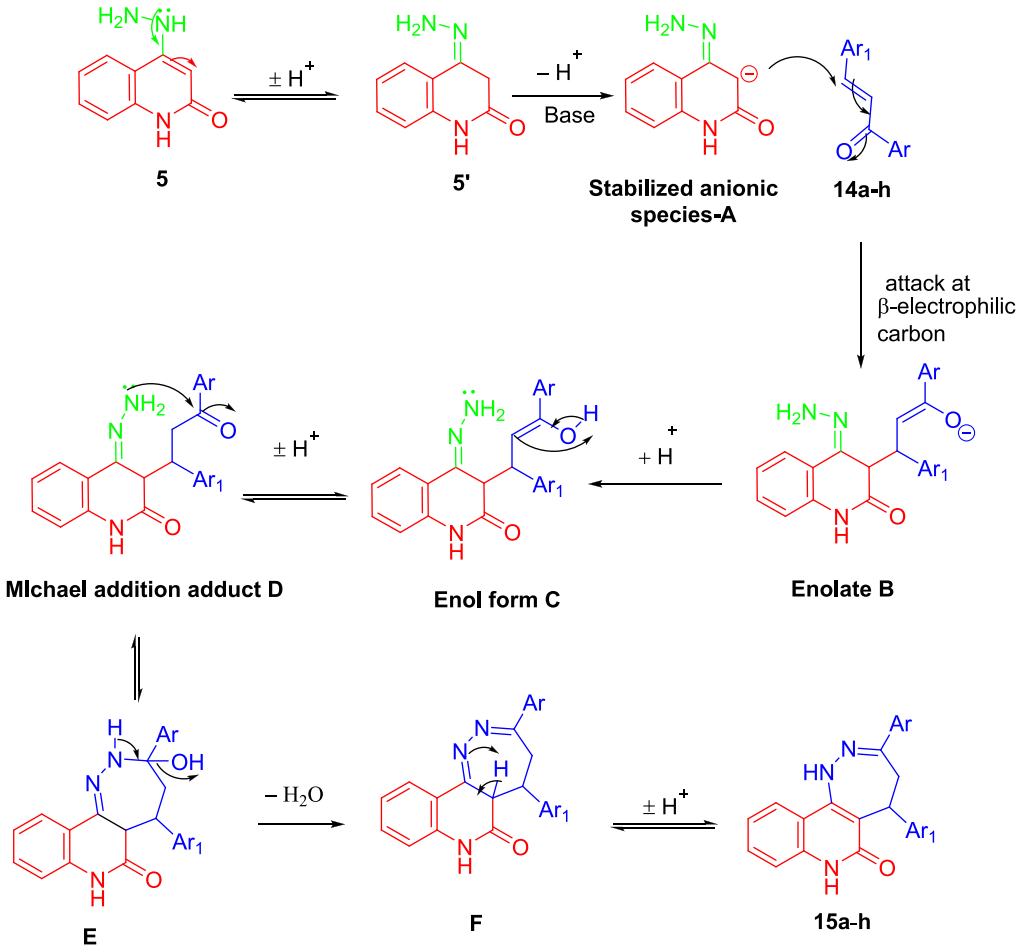

Fig.8. A plausible mechanism for the formation of 3,5-diaryl-1,4,5,7-tetrahydro-6H-[1,2]diazepino[4,3-*c*]quinolin-6-one derivatives 15a-h.

Table 1
GSK-3β inhibitory activity (IC_{50} in **nM**) values of **7a-f, 9a-c**, **11**, **13** and **15a-h** and staurosporine.

Compound	R	R_1	R_2	R_3	IC_{50} (nM) ± SD	Relative potency %
7a	OMe	H	OMe	H	13.98 ± 0.79	36.04 %
7b	OMe	H	H	OMe	21.31 ± 0.51	28.72 %
7c	H	OMe	OMe	H	4.68 ± 0.59*	**130.77 %**
7d	H	OMe	OMe	OMe	32.82 ± 0.86	18.65 %
7e	H	H	OH	H	7.38 ± 0.91*	**82.93 %**
7f	H	OMe	OH	H	8.27 ± 0.60*	**74.00 %**
9a	H	–	–	–	12.88 ± 0.63	47.52 %
9b	Cl	–	–	–	60.30 ± 2.41	10.15 %
9c	Br	–	–	–	29.65 ± 0.85	20.64 %
15a	H	H	–	–	10.65 ± 0.73	**57.46 %**
15b	OMe	H	–	–	27.89 ± 0.76	21.94 %
15c	Cl	H	–	–	14.35 ± 0.52	42.65 %
15d	Br	H	–	–	10.92 ± 0.74	**56.04 %**
15e	H	OMe	–	–	22.39 ± 0.81	27.33 %
15f	OMe	OMe	–	–	23.62 ± 1.71	25.71 %
15 g	Cl	OMe	–	–	95.60 ± 3.12	6.40 %
15 h	Br	OMe	–	–	15.80 ± 0.84	38.73 %
11	–	–	–	–	11.17 ± 0.70	54.79 %
13	–	–	–	–	13.41 ± 0.85	45.63 %
Staurosporine					6.12 ± 0.74	

* $P < 0.05$ for non-significant difference from staurosporine. - Results are the mean values of three separate determinations ± SD.

± 0.74 nM). The structure–activity relationship regarding the three types of targeted structures revealed the following trend: the quinoline-2-one derivatives **7a-f** which were grafted by a hydrophilic tail with polar functionalities, demonstrated noticeably strong inhibitory effect against GSK-3β except for compounds **7b** and **7d** (IC_{50} = 21.31 ± 0.51 and 32.82 ± 0.86 nM, respectively). With an IC_{50} value of 4.68 ± 0.59 nM, compound **7c** demonstrated the most promising GSK-3β inhibitory activity. Moreover, both compounds **7e** (IC_{50} = 7.38 ± 0.91 nM) and **7f** (IC_{50} = 8.27 ± 0.60 nM) exhibited comparable GSK-3β inhibitory activity with reference compound staurosporine (IC_{50} = 6.12 ± 0.74 nM). On the other hand, compound **7d** (IC_{50} = 32.82 ± 0.86 nM) showed an obvious decrease in the activity that may be attributed to the bulkiness and steric hinderance of the trimethoxy substitution.

It was noteworthy that compounds with 1*H*-pyrrol-2,5-dione warhead as in **11** and **13** (IC_{50} = 11.17 ± 0.70 and 13.41 ± 0.85 nM, respectively) or unsubstituted pyrrolidin-2-one warhead as **9a** (IC_{50} = 12.88 ± 0.63 nM) revealed excellent inhibitory activity. However, increase in the lipophilicity of pyrrolidin-2-one warheads by Cl substitution as in **9b** (IC_{50} = 60.30 ± 2.41 nM) or by Br substitution in **9c** (IC_{50} = 29.65 ± 0.85 nM), resulted in a decrease of the enzyme inhibitory action.

Regarding diazepino[4,3-*c*]quinolin-6-one structures, **15a-h** (IC_{50} ranging from 10.65 ± 0.73 to 27.89 ± 0.76 nM), all the compounds revealed good to moderate inhibitory action against GSK-3β apart from **15 g** (IC_{50} = 95.60 ± 3.12 nM) that showed an unanticipated dramatic decline in the activity. The substitution on either of the two phenyl rings exhibited a significant impact on activity. In general, unsubstituted phenyl groups as in **15a** (IC_{50} = 10.65 ± 0.73 nM) or substitution of either two rings with electron withdrawing groups as in **15c** (IC_{50} = 14.35 ± 0.52 nM) and **15d** (IC_{50} = 10.92 ± 0.74 nM) showed improved activity compared with substitution with electron donating groups as in **15b** and **15e** (IC_{50} = 27.89 ± 0.76 and 22.39 ± 0.81 nM, respectively) or substitution on both rings as in **15f**, **15d** and **15 h** (IC_{50} = 23.62 ± 1.71, 95.60 ± 3.12 and 15.80 ± 0.84 nM, respectively). In general, the GSK-3β inhibitory activity of **7c** was the greatest. As a result, **7c** was selected for further investigations.

2.2.2. *Protein tau phosphorylation inhibition*

As previously mentioned, the build-up of hyperphosphorylated tau leads to the formation of NFTs with subsequent neuronal death. Using a homogeneous time resolved fluorescence (HTRF) assay method [52,53], the phosphorylation status of tau and inhibitory effect of **7c**, **7e** and **7f** were assessed at the cellular level. The selective protein phosphatase 2A inhibitor, okadaic acid (OA), causes tau hyperphosphorylation, oligomerization and is widely employed in cell-based models of tauopathy. As a result, we assess the compound's anti-AD potential using an OA-induced neurotoxicity cell model. Tau aggregates levels are expressed in terms of Delta F% and Signal 665/620. As shown in Fig. 9, the decreased Delta F% and Signal 665/620 ratio are associated with reduced aggregated tau load implying that compounds' **7c**, **7e** and **7f** administration considerably reduced aggregated tau.

2.2.3. *Cytotoxicity bioassay*

To verify that the examined compounds are devoid of cytotoxicity, the toxicity induced by certain chemical substances on the human liver or brain cells are investigated. So, the cell viability was then measured using the MTT test [54] before performing *in vivo* testing to assess the safety of compounds **7c, 7e** and **7f**. The results demonstrated compounds' **7c**, **7e** and **7f** low cytotoxicity against healthy human hepatic

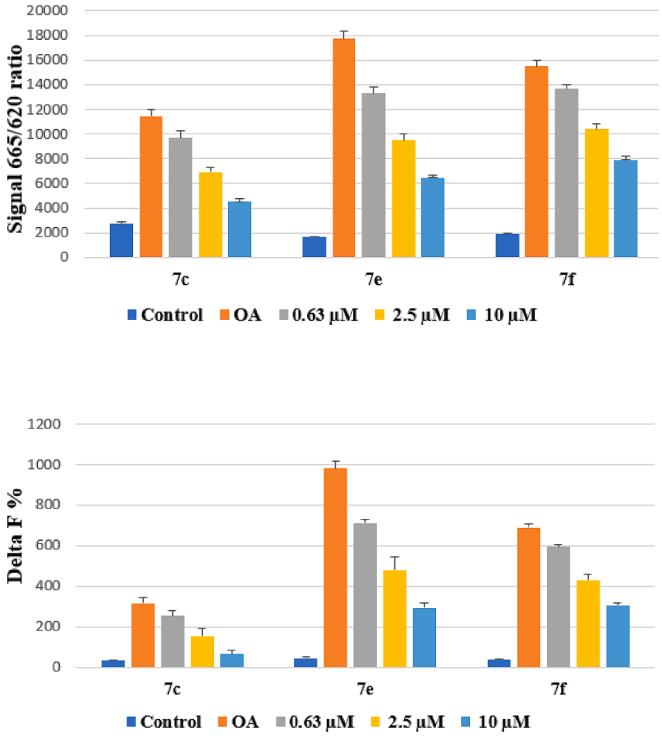

Fig.9. Protective effect of compounds **7c**, **7e** and **7f** against okadaic acid-induced neurotoxicity. Results are the mean values of three separate determinations ± SD.

(THLE2) (IC_{50} ranges between 48.463 ± 2.15 and 74.03 ± 4.27 μM) and neuroblastoma (SHSY5Y) (IC_{50} ranges between 19.42 ± 1.21 and 51.65 ± 2.17 μM) cell lines when compared to staurosporine (IC_{50} = 22.18 ± 1.47 and 12.983 ± 0.77 μM, respectively) as illustrated in Fig. 10.

2.2.4. Kinetic study of GSK-3β inhibition

In order to explore the binding mechanism of the synthesized compounds with GSK-3β binding site, the most effective inhibitor **7c** was chosen for kinetic analysis. As shown in Fig. 11, The reciprocal Lineweaver-Burk plot exhibited rising slopes and the same Y-intercepts as inhibitor concentration increased. This pattern suggested that compound **7c** functioned as a competitive inhibitor of GSK-3β enzyme.

2.2.5. Selectivity profiling of 7c

To assess the selectivity profile for the herein-reported target molecules towards GSK-3β, the most promising quinolinone-based compound **7c** was evaluated at a concentration of 10 μM for its potential inhibitory effect on a small panel of nine GSK-3β off-target kinases; GSK-3α, CK2, CLK1, PKCa, CDK2, CDK5, JNK1, MEKK1, and SAPK2a, as illustrated in Fig. 12.

The findings disclosed that **7c** didn't exert noticeable inhibition toward GSK-3α, CK2, PKCa, and CDK5 (% inhibition < 10), whereas it showed weak inhibitory activity against CDK2, JNK1, MEKK1, and SAPK2a kinases with % inhibition spanning from 13.4 % to 26.8 %. Notably, the most affected kinase was CLK1 with 32.5 % inhibition.

Interestingly, the role of CLK1 is reported in the pathophysiology of Alzheimer's disease, and thus its targeting stands out as a promising therapeutic approach for Alzheimer's disease drug discovery and development [55]. Consequently, compound **7c**'s activity profile, while not highly selective, may provide a starting point and valuable insights into the design of multi-target inhibitors. In other words, the partial promiscuity of compound **7c** may not necessarily be a drawback in the context of AD treatment. The multifactorial nature of AD suggests that a multi-target therapeutic approach could be beneficial. The observed activity of compound **7c** on CLK1 kinase could be leveraged to design multi-target-directed ligands (MTDLs) that simultaneously modulate different pathways implicated in AD pathogenesis. The development of MTDLs is a promising strategy in AD research, as it aligns with the disease's complexity and the need for interventions that can address multiple pathological processes [56].

2.2.6. Behavioral studies in vivo

The most important factor to be considered when evaluating anti-AD drugs is cognitive improvement in AD animal models. Compound **7c**, which shown enhanced GSK-3β inhibitory effectiveness *in vitro* along with little cytotoxicity towards brain and hepatic cell lines, was further evaluated for its capacity to restore impaired memory in AD animal models, which have been administered scopolamine. Passive avoidance test [57] was carried out with donepezil as a positive control using transfer latency time (TLT) in seconds (Fig. 13). Based on the data, mice in the scopolamine model group had a TLT = 251.53, and it was significantly shorter than the control group (TLT = 381.40) ($P < 0.01$). Donepezil-treated mice displayed a statistically significant rise in TLT from 251.53 to 356.27 in comparison to the model group ($P < 0.01$). By administration of compound **7c** to a group of mice, the TLT increased significantly from 251.53 to 327.27 ($P < 0.01$). The findings suggested that compound **7c** which could cross the blood–brain barrier, might reverse scopolamine-induced cognitive impairment.

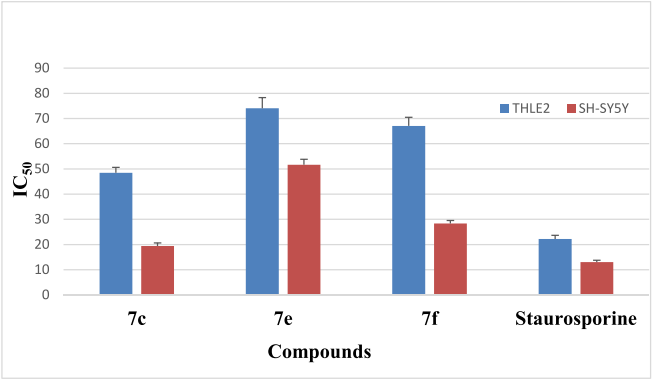

Fig.10. Compounds **7c**, **7e**, **7f** and staurosporine cytotoxicity on neural (red) and hepatic (pink) cell lines. Results are the mean values of three separate determinations ± SD.

2.3. Molecular Modeling study

2.3.1. Molecular docking

Molecular docking simulations were used to investigate the interaction of the most active inhibitors **7c**, **7e**, and **7f** with the GSK-3β kinase domain in order to justify their promising biological action and disclose their likely binding pattern. To that purpose, the protein structure of GSK-3β co-crystallized with indirubin-3′-monoxime inhibitor (IC_{50} = 22 nM) (PDB ID: 1Q41) [58] was retrieved from the protein data bank [https://www.rcsb.org/].

To validate the molecular docking protocol used, the co-crystallized ligand at the GSK-3β active site was first self-docked. The self-docking stage accurately reproduced the co-crystallized ligand's binding pattern, showing that the docking setup used is suitable for the planned simulations. The self-docking exhibited RMSD of 0.262 Å between the docked and co-crystallized ligand poses, and the attained docking pose was able to replicate the key interactions that the co-crystallized ligand achieved with the crucial amino acids in the GSK-3β active site (Hinge region Asp133 and Val135) (Supplementary Fig. S5.5).

A consistent binding pattern was observed by the newly synthesized compounds **7c**, **7e** and **7f** (Fig. 14). The quinolone ring is accommodated in the hinge region interacting through hydrogen bonding by its NH and CO with the backbone CO and NH of the key amino acids Asp133 and Val135, respectively. Moreover, through hydrophobic interaction, the fused benzene ring of the quinolone heterocycle interacts with the hydrophobic side chains of the surrounding amino acids Val70, Ala83, Val110, Leu132, Leu188, and Cys199. Furthermore, compounds **7c** and **7f** perform additional interaction by their peripheral substituted phenyl group as they interact with the nucleotide-binding loop amino acid Arg141 guanidine group that caps the end of the pocket through hydrogen bonding. This extra interaction could rationalize their promising binding scores − 11.17 and − 12.34 kcal/mol, respectively, (Table 2) and their superior biological activity.

2.3.2. Computational prediction of the ADME properties

Molecules cannot be exclusively regarded as therapeutic candidates only because of their excellent pharmacological efficacy and minor toxicological consequences. It is crucial to explore prospective new medications' pharmacokinetic properties as early as possible throughout the process of developing new drugs. Hence, we predicted drug-like capabilities for compounds **7c**, **7e**, and **7f** using SwissADME web tool (https://www.swissadme.ch/) [59]. The results shown in Table 3, demonstrated the tendency of the studied compounds to obey Lipinski's rule [60]. Except for the INSATU (Saturation) property, all the physicochemical parameters of **7c**, **7e** and **7f** were optimal and positioned in the pink zone of the bioavailability radar graph (Supplementary Fig. S5.4.).

2.3.3. Permeation of blood brain barrier (BBB)

Permeability of the blood–brain barrier (BBB) is a critical *in silico* parameter for CNS active drugs that suggests the ability of a chemical to penetrate the BBB into CNS. In this regard, the BBB permeability of compounds **7c**, **7e** and **7f** was estimated using the CBLigand-BBB prediction server [61] and pkCSM [62]. In the CBLigand-BBB predictor,

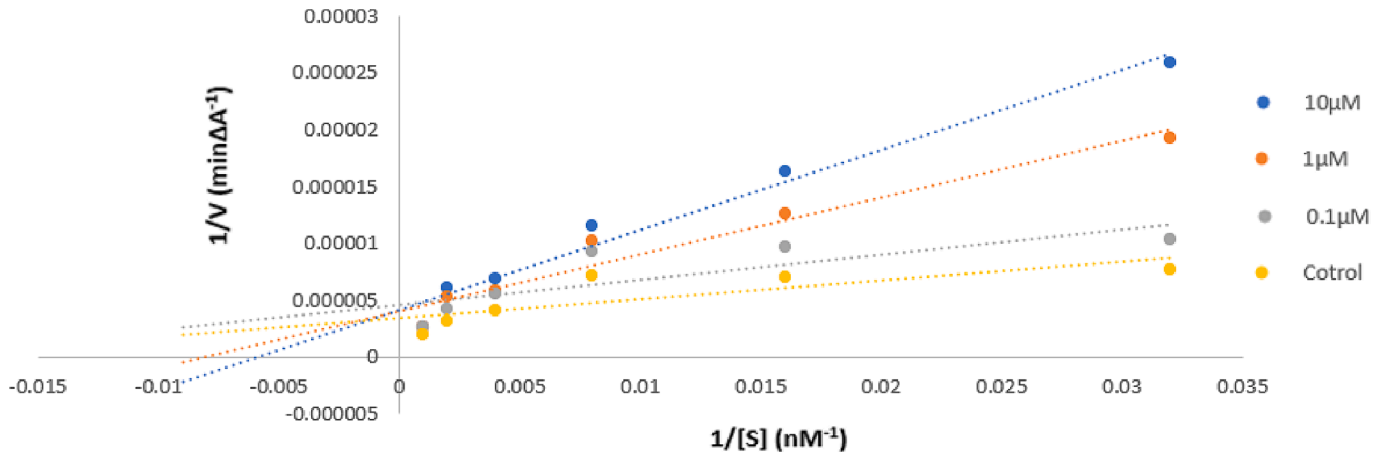

Fig.11. Lineweaver-Burk plot for the GSK-3β assay at different concentrations of **7c.** Results are the mean values of three separate determinations ± SD.

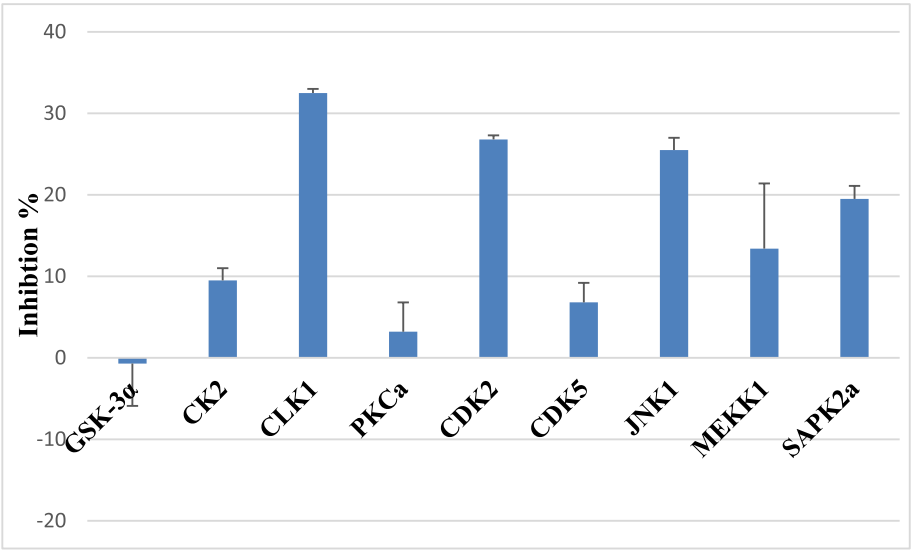

Fig.12. *In vitro* kinase selectivity of compound **7c** (10 μM) against several kinases. Results are the mean values of three separate determinations ± SD.

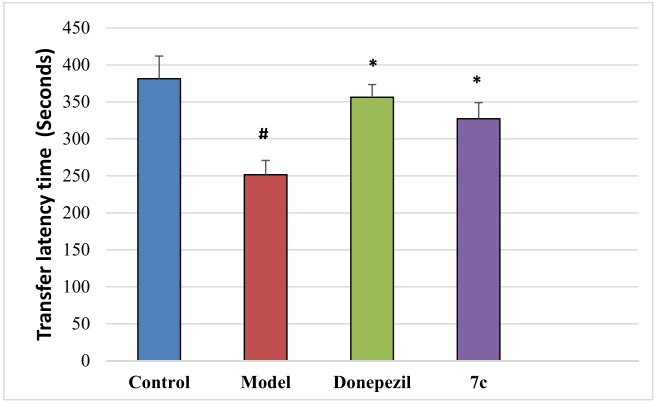

Fig.13. A diagram illustrates the effect of donepezil and compound **7c** on the (TLT) in seconds. (*p < 0.01 vs scopolamine model group while #p < 0.01 vs control group).

four distinct fingerprints are combined with two distinct algorithms, Support Vector Machine (SVM) and AdaBoost, to predict if the synthesized compound will be able (+) or fail (−) to pass the BBB. In the event that the predictor score exceeds zero in each combination, the compound will be able to pass BBB. Table 4 demonstrates that all computations yielded BBB (+), which is pivotal characteristic for AD's targeting compounds. Conversely, BBB permeability and CNS permeability are two *in silico* characteristics provided by the pkCSM server that indicate the compound's potential to traverse the BBB. The first parameter estimates a compound's capacity to pass through the BBB. The second disregards systemic dispersion and is related with direct assessment of brain-blood permeability. The results showed that all the estimated compounds have acceptable BBB and CNS penetration, with optimum log BB values ranging from − 0.180 to − 0.973 (appropriate range is between 0.3 and − 1) and optimal log PS values ranging from − 2.114 to − 2.302 (appropriate range is between − 2 to − 3), respectively.

* A descriptor combination expressed as bit strings. Each bit position accounts for a specific structural feature and the bit is set on, if this feature is present in the molecule. Using various algorithms, a fragmentation scheme program breaks up structures according to atoms, chains, or functional groups (substructure fingerprint), then correlates the fragments with chemical attributes.

3. Conclusion

The results of the previously created multi-protein structure

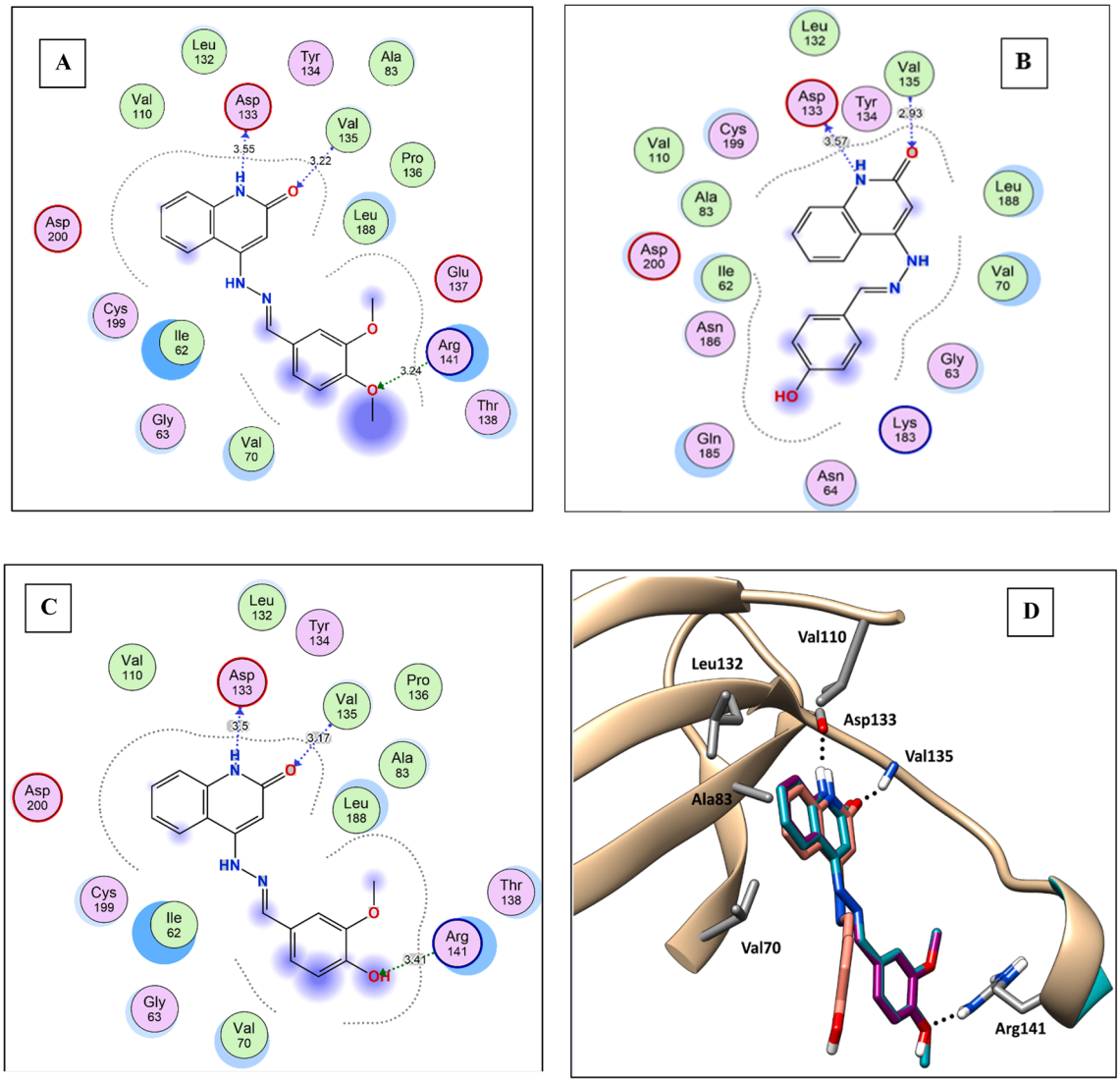

Fig.14. (**A**), (**B**) and (**C**) 2D representations of interactions of compounds **7c**, **7e** and **7f** respectively, with the GSK-3β active site. (**D**) 3D representation of the superimposed docked models of **7c** (cyan), **7e** (salmon) and **7f** (magenta) in GSK-3β active site.

Table 2
Docking energy scores (*S*) (kcal/mol) for the co-crystallized ligand as well as compounds **7c**, **7e**, and **7f** in GSK-3β kinase domain.

Compound	Energy score (S) kcal/mol
7c	−11.17
7e	−10.62
7f	−12.34
Co-crystallized ligand	−12.02

receptor-based 3D pharmacophore model indicated that ZINC67773573 **VIII**, quinolin-2-one derivative, may provide a promising lead for developing novel GSK-3β inhibitors for AD's treatment. Therefore, in this study, a novel series of quinolin-2-one derivatives were synthesized and evaluated for GSK-3β inhibitory activity. *In vitro* screening identified three compounds: **7c**, **7e** and **7f** as promising GSK-3β inhibitors. Compounds **7c**, **7e** and **7f** were found to exhibit superior inhibitory effect on GSK-3β with IC_{50} value ranges between 4.68 ± 0.59 to 8.27 ± 0.60 nM compared to that of staurosporine (IC_{50} = 6.12 ± 0.74 nM). Considerably, compounds **7c**, **7e** and **7f** effectively lowered tau hyperphosphorylated aggregates and proving their safety towards the SH-SY5Y and THLE2 normal cell lines. The most promising compound **7c** alleviated cognitive impairments in the scopolamine-induced model in mice. Compound **7c**'s activity profile, while not highly selective, may provide a starting point and valuable insights into the design of multi-target inhibitors. According to the ADME prediction results,

Table 3
Predicted physicochemical properties for compounds **7c**, **7e** and **7f**.

Comp.	Molecular weight (MW)	octanol/ water partition coefficient (LogP)	Topological polar surface area (tPSA)	H. bond donor (HBD)	H. bond acceptor (HBA)	number of rotatable bonds (Rotor)	Lipinski's Violations
7c	323.35	2.75	75.71 Å^2	2	4	5	0
7e	279.29	2.38	77.48 Å^2	3	3	3	0
7f	309.32	2.43	86.71 Å^2	3	3	4	0

Table 4
BBB scores of compounds **7c**, **7e** and **7f** were calculated using the CBLigand-BBB prediction system.

Fingerprints*	Calculated BBB score					
	7c		**7e**		**7f**	
	AdaBoost algorithm	**SVM algorithm**	**AdaBoost algorithm**	**SVM algorithm**	**AdaBoost algorithm**	**SVM algorithm**
MACCSFP	2.046	0.056	4.085	0.106	0.793	0.043
OpenbabelFP2	6.105	0.146	0.519	0.129	3.682	0.144
Molprint 2D	5.485	0.250	1.831	0.082	1.029	0.065
PubChem	21.523	0.305	14.481	0.158	20.032	0.273

compounds **7c**, **7e** and **7f** followed Lipinski's rule of five and could almost permeate the BBB. Molecular docking simulations showed that these compounds are accommodated in the ATP binding site interacting by their quinoline-2-one ring through hydrogen bonding to the key amino acids Asp133 and Val135 at the hinge region. The findings of this study could aid in the discovery and development of potential GSK-3β inhibitors as anti-AD medicines.

4. Experimental

4.1. Chemistry

2,4-Dichloroquinoline **3** [36], 4-Chloroquinolin-2(1*H*)-one **4** [37,38], 4-Hydrazineylquinolin-2(1*H*)-one **5** [39,40] are prepared in accordance with the reported procedures. The findings of the instruments and thermal analyses are presented in the supporting data (Supplementary S5.1).

4.1.1. General procedures for synthesis of compounds7a-f and 9a-c

A mixture of hydrazide **5** (1 mmol, 175.1 mg) and (1 mmol) of the appropriate benzaldehyde derivative **6a-f** or 1*H*-indole-2,3-dione derivative **8a-c** in absolute ethanol (15 mL) containing 5 drops of glacial acetic acid was refluxed for 24–48 h. The formed solid was filtered off and washed with hot ethanol to yield the corresponding pure hydrazone derivatives **7a-f** and **9a-c**, respectively.

4.1.1.1. (E)-4-[2-(2,4-dimethoxybenzylidene)hydrazinyl]quinolin-2(1H)-one (7a). Brown beige powder, 92 % yield; m.p.: 296–298 °C; IR (υ_{max}, cm^{-1}): 3217 & 3156 (2NH), 3090 (CH-Ar.), 2994 (CH aliph.), 1636 (C═O); ^{1}H NMR (DMSO-d_6, 400 MHz): δ 3.83 (s, 3H, OCH_3), 3.88 (s, 3H, OCH_3), 6.20 (s, 1H, C^{3}H-quinolone), 6.64 (d, J = 7.5 Hz, 2H, Ar-Hs), 7.17 (t, J = 7.6 Hz, 1H, Ar-H), 7.30 (d, J = 8.1 Hz, 1H, Ar-H), 7.49 (t, J = 7.6 Hz, 1H, Ar-H), 7.86 (d, J = 9.0 Hz, 1H, Ar-H), 8.07 (d, J = 8.1 Hz, 1H, Ar-H), 8.67 (s, 1H, CH = *N*), 10.65 (s, 1H, NH exchanged with D_2O), 11.01 (s, 1H, NH exchanged with D_2O); ^{13}C NMR (DMSO-d_6, 100 MHz): δ 55.88 (OCH_3), 56.21 (OCH_3), 93.89 (C^{3}H-quinolone), 98.76, 106.95, 112.36, 116.10, 121.13, 122.37, 126.80, 130.75, 139.84, 140.00 (HC = *N*), 148.91, 159.13 (C—O), 162.43 (C—O), 163.40 (C═O); Anal. Calcd for $C_{18}H_{17}N_3O_3$ (323.35): C, 66.86; H, 5.30; N, 13.00. Found: C, 67.05; H, 5.43; N, 13.21.

4.1.1.2. (E)-4-[2-(2,5-dimethoxybenzylidene)hydrazinyl]quinolin-2(1H)-one (7b). Off-white crystals, 94 % yield; m.p.: 295–297 °C; IR (υ_{max}, cm^{-1}): 3213 & 3163 (2NH), 3078 (CH-Ar.), 2994 (CH aliph.), 1632 (C═O); ^{1}H NMR (DMSO-d_6, 400 MHz): δ 3.78 (s, 3H, OCH_3), 3.83 (s, 3H, OCH_3), 6.25 (s, 1H, C^{3}H-quinolone), 6.97 (dd, J = 3.0 & 9.0 Hz, 1H, Ar-H), 7.05 (d, J = 9.0 Hz, 1H, Ar-H), 7.18 (t, J = 7.5 Hz, 1H, Ar-H), 7.31 (d, J = 8.2 Hz, 1H, Ar-H), 7.44 (d, J = 2.9 Hz, 1H, Ar-H), 7.50 (t, J = 7.6 Hz, 1H, Ar-H), 8.09 (d, J = 8.0 Hz, 1H, Ar-H), 8.73 (s, 1H, CH = *N*), 10.82 (s, 1H, NH exchanged with D_2O), 11.1 (s, 1H, NH exchanged with D_2O); ^{13}C NMR (DMSO-d_6, 100 MHz): δ 55.88 (OCH_3), 56.68 (OCH_3), 94.47 (C^{3}H-quinolone), 109.39, 112.31, 113.84, 116.17, 117.29, 121.21, 122.40, 123.85, 130.85, 139.62, 139.85 (HC = *N*), 148.81, 152.30 (C—O), 153.83 (C—O), 163.33 (C═O); Anal. Calcd for $C_{18}H_{17}N_3O_3$ (323.35): C, 66.86; H, 5.30; N, 13.00. Found: C, 66.95; H, 5.42; N, 13.17.

4.1.1.3. (E)-4-[2-(3,4-dimethoxybenzylidene)hydrazinyl]quinolin-2(1H)-one (7c). Brown beige powder, 98 % yield; m.p.: 287–289 °C; IR (υ_{max}, cm^{-1}): 3202 and 3167 (2NH), 3075 (CH-Ar.), 2990 (CH aliph.), 1632 (C═O); ^{1}H NMR (DMSO-d_6, 400 MHz): δ 3.81 (s, 3H, OCH_3), 3.85 (s, 3H, OCH_3), 6.25 (s, 1H, C^{3}H-quinolone), 7.02 (d, J = 8.3 Hz, 1H, Ar-H), 7.17–7.22 (m, 2H, Ar-Hs), 7.31 (d, J = 8.1 Hz, 1H, Ar-H), 7.38 (d, J = 1.5 Hz, 1H, Ar-H), 7.50 (t, J = 7.6 Hz, 1H, Ar-H), 8.06 (d, J = 8.1 Hz, 1H, Ar-H), 8.32 (s, 1H, CH = *N*), 10.66 (s, 1H, NH exchanged with D_2O), 11.06 (s, 1H, NH exchanged with D_2O); ^{13}C NMR (DMSO-d_6, 100 MHz): δ 55.90 (OCH_3), 56.03 (OCH_3), 94.18 (C^{3}H-quinolone), 108.46, 112.05, 112.36, 116.19, 121.15, 121.60, 122.40, 127.94, 130.83, 139.83, 144.54 (HC = *N*), 148.90, 149.61 (C—O), 150.80 (C—O), 163.40 (C═O); Anal. Calcd for $C_{18}H_{17}N_3O_3$ (323.35): C, 66.86; H, 5.30; N, 13.00. Found: C, 67.14; H, 5.47; N, 13.26.

4.1.1.4. (E)-4-[2-(3,4,5-trimethoxybenzylidene)hydrazinyl]quinolin-2(1H)-one (7d). Off-white crystals, 98 % yield; m.p.: 283–285 °C; IR (υ_{max}, cm^{-1}): 3298 & 3160 (2NH), 3090 (CH-Ar.), 2974 (CH aliph.), 1640 (C═O); ^{1}H NMR (DMSO-d_6, 400 MHz): δ 3.71 (s, 3H, OCH_3), 3.86 (s, 6H, 2 OCH_3), 6.31 (s, 1H, C^{3}H-quinolone), 7.04 (s, 2H, Ar-Hs), 7.19 (t, J = 7.5 Hz, 1H, Ar-H), 7.33 (d, J = 8.2 Hz, 1H, Ar-H), 7.51 (t, J = 7.5 Hz, 1H, Ar-H), 8.09 (d, J = 8.1 Hz, 1H, Ar-H), 8.32 (s, 1H, CH = *N*), 10.81 (s, 1H, NH exchanged with D_2O), 11.19 (s, 1H, NH exchanged with D_2O); ^{13}C NMR (DMSO-d_6, 100 MHz): δ 56.36 (2 OCH_3), 60.58 (OCH_3), 94.47 (C^{3}H-quinolone), 104.25, 112.35, 116.27, 121.27, 122.45, 130.68, 130.92, 139.28, 139.79 (HC = *N*), 144.31, 148.96 (C—O), 153.69 (2C-O), 163.54 (C═O); MS *m/z* (%): 353.24 (M^+, 11.57), 349.21 (100); Anal. Calcd for $C_{19}H_{19}N_3O_4$ (353.38): C, 64.58; H, 5.42; N, 11.89. Found: C, 64.79; H, 5.60; N, 12.05.

4.1.1.5. (E)-4-[2-(4-hydroxybenzylidene)hydrazinyl]quinolin-2(1H)-one (7e). Off-white crystals, 95 % yield; m.p.: 310–312 °C; IR (υ_{max}, cm^{-1}): 3630 (phenolic OH), 3414 and 3345 (2NH), 3086 (CH-Ar.), 1640 (C═O); ^{1}H NMR (DMSO-d_6, 400 MHz): δ 6.24 (s, 1H, C^{3}H-quinolone), 6.87 (d, J = 8.5 Hz, 2H, Ar-Hs), 7.18 (t, J = 7.5 Hz, 1H, Ar-H), 7.33 (d, J = 8.2 Hz, 1H, Ar-H), 7.50 (t, J = 7.6 Hz, 1H, Ar-H), 7.59 (d, J = 8.5 Hz, 2H, Ar-Hs), 8.07 (d, J = 8.1 Hz, 1H, Ar-H), 8.31 (s, 1H, CH = *N*), 9.94 (s, 1H, OH exchanged with D_2O), 10.62 (s, 1H, NH exchanged with D_2O), 11.11 (s, 1H, NH exchanged with D_2O); ^{13}C NMR(DMSO-d_6, 100 MHz): δ 93.87 (C^{3}H-quinolone), 112.40, 116.24, 121.19, 122.39, 126.20, 128.82, 130.82, 139.81, 144.78 (HC = *N*), 149.08, 159.47 (C—O), 163.55 (C═O); Anal. Calcd for $C_{16}H_{13}N_3O_2$ (279.30): C, 68.81; H, 4.69; N, 15.05. Found: C, 69.07; H, 4.82; N, 15.23.

4.1.1.6. (E)-4-[2-(4-hydroxy-3-methoxybenzylidene)hydrazinyl]quinolin-2(1H)-one (7f). Off white crystals, 81 % yield; m.p.: 280–282 °C; IR (υ_{max}, cm^{-1}): 3557 (phenolic OH), 3283 & 3260 (2NH), 3086 (CH-Ar.), 2967 (CH aliph.), 1639 (C═O); ^{1}H NMR (DMSO-d_6, 400 MHz): δ 3.86 (s, 3H, OCH_3), 6.24 (s, 1H, C^{3}H-quinolone), 6.86 (d, J = 8.1 Hz, 1H, Ar-H), 7.11 (dd, J = 1.4, 8.1 Hz, 1H, Ar-H), 7.19 (t, J = 7.6 Hz, 1H, Ar-H), 7.32 (d, J = 8.2 Hz, 1H, Ar-H), 7.36 (d, J = 1.3 Hz, 1H, Ar-H), 7.50 (t, J = 7.6 Hz, 1H, Ar-H), 8.07 (d, J = 8.1 Hz, 1H, Ar-H), 8.30 (s, 1H, CH = *N*), 9.52 (s, 1H, OH exchanged with D_2O), 10.62 (s, 1H, NH exchanged with D_2O), 11.08 (s, 1H, NH exchanged with D_2O); ^{13}C NMR (DMSO-d_6, 100 MHz): δ 56.01 (OCH_3), 93.94 (C^{3}H-quinolone), 109.21, 112.39, 116.00,

116.21, 121.16, 121.88, 122.40, 126.62, 130.82, 139.82 (HC = *N*), 144.96, 148.56 (C—O), 149.02 (C—O), 163.49 (C═O); Anal. Calcd for $C_{17}H_{15}N_3O_3$ (309.33): C, 66.01; H, 4.89; N, 13.58. Found: C, 66.23; H, 5.03; N, 13.80.

4.1.1.7. (Z)-4-[2-(2-oxoindolin-3-ylidene)hydrazinyl]quinolin-2(1H)-one (9a). Dark brown powder, 99 % yield; m.p.: 342–344 °C; IR (υ_{max}, cm^{-1}): 3368 & 3132 (3NH), 3075 (CH-Ar.), 2994 (CH aliph.), 1690 & 1651 (2C = O); ^{1}H NMR (DMSO-d_6, 400 MHz): δ 6.53 (s, 1H, C^3H-quinolone), 6.97 (d, J = 7.8 Hz, 1H, Ar-H), 7.11 (t, J = 7.5 Hz, 1H, Ar-H), 7.29–7.39 (m, 3H, Ar-Hs), 7.54–7.60 (m, 2H, Ar-Hs), 7.67 (d, J = 7.4 Hz, 1H, Ar-H), 11.35 (s, 1H, NH exchanged with D_2O), 11.45 (s, 1H, NH exchanged with D_2O), 13.38 (s, 1H, NH exchanged with D_2O); ^{13}C NMR (DMSO-d_6,100 MHz): δ 97.36 (C^3H-quinolone) 111.52, 111.73, 116.67, 120.34, 120.51, 120.63, 122.28, 122.95, 131.05, 131.55, 134.55, 139.95, 141.86, 146.44 (C═N-NH), 162.74 (C═O), 164.14 (C═O); MS *m/z* (%): 304.60 (M^+, 12.52), 129.90 (1 0 0); Anal. Calcd for $C_{17}H_{12}N_4O_2$ (304.31): C, 67.10; H, 3.97; N, 18.41. Found: C, 66.89; H, 4.15; N, 18.63.

4.1.1.8. (Z)-4-[2-(5-chloro-2-oxoindolin-3-ylidene)hydrazinyl]quinolin-2 (1H)-one (9b). Yellow powder, 93 % yield; m.p.: 365–367 °C; IR (υ_{max}, cm^{-1}):3360 & 3159 (3NH), 3059 (CH-Ar.), 2997 (CH aliph.), 1690 & 1643 (2C = O); ^{1}H NMR (DMSO-d_6, 400 MH): δ 6.62 (s, 1H, C^3H-quinolone), 6.98 (d, 1H, J = 8.3 Hz, Ar-H), 7.31 (t, J = 7.6 Hz 1H, Ar-H), 7.37–7.40 (m, 2H, Ar-Hs), 7.53–7.61 (m, 2H, Ar-Hs), 7.72 (s, 1H, Ar-H), 11.45 (s, 1H, NH exchanged with D_2O), 11.48 (s, 1H, NH exchanged with D_2O), 13.35 (s, 1H, NH exchanged with D_2O); ^{13}C NMR (DMSO-d_6,100 MHz): δ 98.08 (C^3H-quinolone), 111.70, 112.99, 116.70, 120.33, 122.28, 122.36, 127.20, 130.35, 131.63, 133.46, 139.94, 140.43, 146.27 (C═N-NH), 162.73 (C═O), 163.99 (C═O); Anal. Calcd for $C_{17}H_{11}ClN_4O_2$ (338.75): C, 60.28; H, 3.27; N, 16.54. Found: C, 60.43; H, 3.40; N, 16.81.

4.1.1.9. (Z)-4-[2-(5-bromo-2-oxoindolin-3-ylidene)hydrazinyl]quinolin-2 (1H)-one (9c). Yellow powder, 95 % yield; m.p.: 372–374 °C; IR (υ_{max}, cm^{-1}): 3348 & 3159 (3NH), 3055 (CH-Ar.), 2951 (CH aliph.), 1690 & 1643 (2C = O); ^{1}H NMR (DMSO-d_6, 400 MHz): δ 6.62 (s, 1H, C^3H-quinolone), 6.93 (d, J = 8.2 Hz, 1H, Ar-H), 7.31 (t, J = 7.3 Hz, 1H, Ar-H), 7.38 (d, J = 8.0 Hz, 1H, Ar-H), 7.49–7.61 (m, 3H, Ar-Hs), 7.85 (s, 1H, Ar-H), 11.45 (s, 1H,NH exchanged with D_2O), 11.48 (s, 1H, NH exchanged with D_2O), 13.34 (s, 1H, NH exchanged with D_2O); ^{13}C NMR (DMSO-d_6,100 MHz): δ 98.10 (C^3H-quinolone), 111.68, 113.39, 114.83, 116.67, 120.28, 122.28, 122.66, 123.01, 131.55, 133.07, 133.22, 139.94, 140.77, 146.18 (C═N-NH), 162.68 (C═O), 163.80 (C═O); Anal. Calcd for $C_{17}H_{11}BrN_4O_2$ (383.21): C, 53.28; H, 2.89; N, 14.62. Found: C, 53.47; H, 3.06; N, 14.87.

4.1.2. General procedures for synthesis of compounds 11 and 13

To a solution of hydrazide **5** (10 mmol) in glacial acetic acid (25 mL) and anhydrous sodium acetate (10 mmol), the appropriate anhydride (10 mmol) **10** or **12** and was added. The reaction mixture was heated under reflux for 24 h. The solution was cooled down to room temperature and poured on iced water to yield the corresponding derivatives **11** and **13**, respectively. The obtained solids were washed with hot glacial acetic acid to afford the pure products.

4.1.2.1. 2-[(2-Oxo-1,2-dihydroquinolin-4-yl)amino]isoindoline-1,3-dione (11). Off-white crystals, 92 % yield; m.p.: 318–320 °C; IR (υ_{max}, cm^{-1}): 3480 & 3310 (2NH), 3086 (CH-Ar.), 2997 (CH aliph.), 1790, 1732 & 1651 (3C = O); ^{1}H NMR (DMSO-d_6, 400 MHz): δ 5.43 (s, 1H, C^3H-quinolone), 7.25 (t, J = 7.6 Hz,1H, Ar-H), 7.34 (d, J = 8.1 Hz, 1H, Ar-H), 7.56 (t, J = 7.5 Hz, 1H, Ar-H), 7.96–8.03 (m, 5H, Ar-Hs), 9.64 (s, 1H, NH exchanged with D_2O), 11.21 (s, 1H, NH exchanged with D_2O); ^{13}C NMR (DMSO-d_6,100 MHz): δ 94.50 (C^3H-quinolone), 112.05, 116.28, 121.65, 122.53, 124.29, 129.91, 131.39, 135.78, 139.63, 150.85, 162.91 (C═O), 166.10 (2C = O); Anal. Calcd for $C_{17}H_{11}N_3O_3$ (305.29): C, 66.88; H, 3.63; N, 13.76. Found: C, 66.71; H, 3.80; N, 14.03.

4.1.2.2. 1-[(2-Oxo-1,2-dihydroquinolin-4-yl)amino]pyrrolidine-2,5-dione (13). Brown beige powder, 82 % yield; m.p.: 333–335 °C; IR (υ_{max}/cm^{-1}): 3352 & 3287 (2NH), 3098 (CH-Ar.), 2994 (CH aliph.), 1713 & 1643 (3C = O); ^{1}H NMR (DMSO-d_6, 400 MHz): δ 1.98 & 2.88 (2 s, 4H, *cis/trans conformers of* $2CH_2$ of pyrrolidine), 5.41 & 5.49 (2 s, 1H, *cis/trans conformers of* C^3H-quinolone), 7.14 & 7.20 (2 t, J = 8.0, 7.3 Hz, 1H, Ar-H), 7.26 & 7.31(2d, J = 7.8, 7.9 Hz, 1H, Ar-H), 7.48 & 7.53 (2 t, J = 7.7, 7.3 Hz, 1H, Ar-H), 7.94 (d, J = 7.6 Hz, 1H, Ar-H), 8.84 & 9.37 (2 s, 1H, *cis/trans conformers of* NH exchanged with D_2O), 10.96 & 11.13 (2 s, 1H, *cis/trans conformers of* NH exchanged with D_2O); ^{13}C NMR (DMSO-d_6,100 MHz): δ 27.08 (pyrrolidine CH_2), 94.47 (C^3H-quinolone), 112.19, 116.16, 121.48, 122.67, 131.19, 139.54, 150.13, 163.08 (C═O),175.40 (2C = O); MS *m/z* (%): 257.52 (M^+, 14.54), 43.10 (1 0 0); Anal. Calcd for $C_{13}H_{11}N_3O_3$ (257.25): C, 60.70; H, 4.31; N, 16.33. Found: C, 60.85; H, 4.43; N, 16.61.

4.1.3. General procedures for synthesis of compounds 15a-h

To a mixture of hydrazide **5** (3.1 mmol) and the respective chalcone derivative **14a-h** (4.5 mmol) in absolute methanol (20 mL), anhydrous potassium carbonate (1 mmol) was added. The resulting reaction mixture was heated under reflux for 30–48 h. The solids thus precipitated were filtered and washed with hot methanol to afford pure products **15a-h.**

4.1.3.1. 3,5-Diphenyl-1,4,5,7-tetrahydro-6H-[1,2]diazepino[4,3-c]quinolin-6-one (15a). Off-white crystals, 65 % yield; m.p.: 288–290 °C; IR (υ_{max}, cm^{-1}): 3441 & 3264 (2NH), 3059 (CH-Ar.), 2951 (CH aliph.), 1651 (C═O); ^{1}H NMR (DMSO-d_6, 400 MHz): δ 3.10 (d, J = 13.6 Hz, 1H, CH of diazepine), 3.64 (dd, J = 5.6, 13.84 Hz, 1H, CH of diazepine), 5.15 (d, J = 3.9 Hz, 1H, CH of diazepine), 7.01 (s, 1H, Ar-H), 7.11 (s, 3H, Ar-Hs), 7.20 (s, 4H, Ar-Hs), 7.30 (d, J = 9.0 Hz, 3H, Ar-Hs), 7.49 (t, J = 7.2 Hz, 2H, Ar-Hs), 8.32 (d, J = 8.1 Hz, 1H, Ar-H), 10.31 (s, 1H, NH exchanged with D_2O), 11.26 (s, 1H, NH exchanged with D_2O); ^{13}C NMR (DMSO-d_6,100 MHz): δ 38.23 (diazepine CH), 42.88 (diazepine CH_2), 109.8, 113.85, 115.97, 121.68, 122.40, 126.20, 126.27, 128.16, 128.18, 128.26, 128.38, 130.19, 138.09, 139.55, 144.57, 145.37, 155.49, 161.88 (C═O); Anal. Calcd for $C_{24}H_{19}N_3O$ (365.44): C, 78.88; H, 5.24; N, 11.50. Found: C, 78.69; H, 5.48; N, 11.65.

4.1.3.2. 3-(4-Methoxyphenyl)-5-phenyl-1,4,5,7-tetrahydro-6H-[1,2]diazepino[4,3-c]quinolin-6-one (15b). Off-white crystals, 65 % yield; m.p.: 283–285 °C; IR (υ_{max}, cm^{-1}): 3437 & 3248 (2NH), 3059 (CH-Ar.), 2955 (CH aliph.), 1651 (C═O); ^{1}H NMR (DMSO-d_6, 400 MHz): δ 3.07 (d, J = 13.6 Hz, 1H, CH of diazepine), 3.61 (dd, J = 5.6, 13.7 Hz, 1H, CH of diazepine), 3.70 (s, 3H, OCH_3), 5.11 (d, J = 4.4 Hz, 1H, CH of diazepine), 6.73 (d, J = 8.4 Hz, 2H, Ar-Hs), 7.00 (d, J = 5.2 Hz, 1H, Ar-H), 7.11 (br. s, 3H, Ar-Hs), 7.19 (t, J = 7.6 Hz, 1H, Ar-H), 7.30 (d, J = 8.0 Hz, 3H, Ar-Hs), 7.48 (t, J = 7.2 Hz, 2H, Ar-Hs), 8.32 (d, J = 8.1 Hz, 1H, Ar-H), 10.17 (s, 1H, NH exchanged with D_2O), 11.22 (s, 1H, NH exchanged with D_2O); ^{13}C NMR (DMSO-d_6, 100 MHz): δ 37.91 (diazepine CH), 42.91 (diazepine CH_2), 55.50 (OCH_3), 109.27, 113.62, 113.89, 115.96, 121.62, 122.35, 126.14, 127.71, 128.09, 128.21, 130.12, 131.91, 138.07, 144.68, 145.36, 155.85, 159.84, 161.90 (C═O); MS *m/z* (%): 395.12 (M^+, 8.52), 326.30 (1 0 0); Anal. Calcd for $C_{25}H_{21}N_3O_2$ (395.46): C, 75.93; H, 5.35; N, 10.63. Found: C, 75.81; H, 5.52; N, 10.89.

4.1.3.3. 3-(4-Chlorophenyl)-5-phenyl-1,4,5,7-tetrahydro-6H-[1,2]diazepino[4,3-c]quinolin-6-one (15c). Off-white crystals, 61 % yield; m.p.: 308–310 °C; IR (υ_{max}, cm^{-1}): 3441 & 3298 (2NH), 3063 (CH-Ar.), 2982 (CH aliph.), 1647 (C═O); ^{1}H NMR (DMSO-d_6, 400 MHz): δ 3.08 (d, J = 12.5 Hz, 1H, CH of diazepine), 3.65 (dd, J = 6.0, 14.0 Hz, 1H, CH of diazepine), 5.15 (d, J = 4.4 Hz, 1H, CH of diazepine), 6.99–7.03 (m, 1H,

Ar-H), 7.07–7.12 (m, 4H, Ar-Hs), 7.19 (d, J = 7.3 Hz, 1H, Ar-H), 7.22–7.26 (m, 2H, Ar-Hs), 7.29 (d, J = 8.0 Hz, 1H, Ar-H), 7.35 (d, J = 8.6 Hz, 2H, Ar-Hs), 7.50 (t, J = 7.6 Hz, 1H, Ar-H), 8.30 (d, J = 8.4 Hz, 1H, Ar-H), 10.36 (s, 1H, NH exchanged with D_2O), 11.28 (s, 1H, NH exchanged with D_2O); ^{13}C NMR (DMSO-d_6, 100 MHz): δ 37.97 (diazepine CH), 42.77 (diazepine CH_2), 110.09, 113.79, 115.99, 121.71, 122.37, 126.25, 127.96, 128.11, 128.19, 128.30, 130.25, 133.36, 138.08, 138.33, 144.46, 145.17, 154.21, 161.82 (C═O); Anal. Calcd for $C_{24}H_{18}ClN_3O$ (399.88): C, 72.09; H, 4.54; N, 10.51. Found: C, 71.84; H, 4.63; N, 10.70.

4.1.3.4. 3-(4-Bromophenyl)-5-phenyl-1,4,5,7-tetrahydro-6H-[1,2]diazepino[4,3-c]quinolin-6-one (15d). Dark brown powder, 58 % yield; m.p.: 299–301 °C; IR (υ_{max}, cm^{-1}): 3441& 3302 (2NH), 3059 (CH-Ar.), 2982 (CH aliph.), 1651 (C═O); ^{1}H NMR (DMSO-d_6, 400 MHz): δ 3.08 (d, J = 14.0 Hz, 1H, CH of diazepine), 3.64 (dd, J = 6.0, 14.1 Hz, 1H, CH of diazepine), 5.15 (d, J = 4.3 Hz, 1H, CH of diazepine), 7.00–7.03 (m, 1H, Ar-H), 7.07–7.13 (m, 4H, Ar-Hs), 7.20 (t, J = 7.5 Hz, 1H, Ar-H), 7.27–7.30 (m, 3H, Ar-Hs), 7.38 (d, J = 8.6 Hz, 2H, Ar-Hs), 7.50 (t, J = 7.5 Hz, 1H, Ar-H), 8.30 (d, J = 8.2 Hz, 1H, Ar-H), 10.37 (s, 1H, NH exchanged with D_2O), 11.28 (s, 1H, NH exchanged with D_2O); ^{13}C NMR (DMSO-d_6, 100 MHz): δ 42.76 (diazepine CH_2), 110.13, 113.79, 121.71, 122.11, 122.37, 126.26, 128.10, 128.20, 128.24, 130.25, 131.22, 138.08, 138.71, 144.44, 145.16, 154.18, 161.82 (C═O); Anal. Calcd for $C_{24}H_{18}BrN_3O$ (444.33): C, 64.88; H, 4.08; N, 9.46. Found: C, 64.95; H, 4.21; N, 9.68.

4.1.3.5. 5-(4-Methoxyphenyl)-3-phenyl-1,4,5,7-tetrahydro-6H-[1,2]diazepino[4,3-c]quinolin-6-one (15e). Off-white crystals, 89 % yield; m.p.: 298–300 °C; IR (υ_{max}, cm^{-1}): 3445 & 3314 (2NH), 3098 (CH-Ar.), 2955 (CH aliph.), 1651 (C═O); ^{1}H NMR (DMSO-d_6, 400 MHz): δ 3.06 (d, J = 13.6 Hz, 1H, CH of diazepine), 3.60 (br. s, 4H, CH of diazepine + OCH_3), 5.09 (d, J = 4.6 Hz, 1H, CH of diazepine), 6.67 (d, J = 8.4 Hz, 2H, Ar-Hs), 7.02 (d, J = 8.4 Hz, 2H, Ar-Hs), 7.18–7.22 (m, 4H, Ar-Hs), 7.29 (d, J = 8.1 Hz, 1H, Ar-H), 7.35–7.37 (m, 2H, Ar-Hs), 7.49 (t, J = 7.6 Hz, 1H, Ar-H), 8.31 (d, J = 8.3 Hz, 1H, Ar-H), 10.28 (s, 1H, NH exchanged with D_2O), 11.25 (s, 1H, NH exchanged with D_2O); ^{13}C NMR (DMSO-d_6, 100 MHz): δ 38.32 (diazepine CH), 41.91 (diazepine CH_2), 55.38 (OCH_3), 110.43, 113.60, 113.87, 115.94, 121.65, 122.38, 126.33, 128.32, 128.62, 129.15, 130.14, 137.54, 138.06, 139.68, 144.40, 155.32, 157.76, 161.84 (C═O); Anal. Calcd for $C_{25}H_{21}N_3O_2$ (395.46): C, 75.93; H, 5.35; N, 10.63. Found: C, 75.69; H, 5.41; N, 10.87.

4.1.3.6. 3,5-Bis(4-methoxyphenyl)-1,4,5,7-tetrahydro-6H-[1,2]diazepino[4,3-c]quinolin-6-one (15f). Off-white crystals, 89 % yield; m.p.: 310–312 °C; IR (υ_{max}, cm^{-1}): 3433 & 3306 (2NH), 3098 (CH-Ar.), 2955 (CH aliph.), 1651 (C═O); ^{1}H NMR (DMSO-d_6, 400 MHz): δ 3.03 (d, J = 13.6 Hz, 1H, CH of diazepine), 3.60 (br. s, 4H, CH of diazepine + OCH_3), 3.71 (s, 3H, OCH_3), 5.06 (d, J = 2.9 Hz, 1H, CH of diazepine), 6.66 (d, J = 7.9 Hz, 2H, Ar-Hs), 6.76 (d, J = 8.1 Hz, 2H, Ar-Hs), 7.03 (d, J = 7.8 Hz, 2H, Ar-Hs), 7.19 (t, J = 7.1 Hz, 1H, Ar-H), 7.28–7.35 (m, 3H, Ar-Hs), 7.48 (t, J = 7.1 Hz, 1H, Ar-H), 8.33 (d, J = 8.0 Hz, 1H, Ar-H), 10.17 (s, 1H, NH exchanged with D_2O), 11.23 (s, 1H, NH exchanged with D_2O); ^{13}C NMR (DMSO-d_6, 100 MHz): δ 38.00 (diazepine CH), 41.97 (diazepine CH_2), 55.35 (OCH_3), 55.50 (OCH_3), 109.82, 113.54, 113.68, 113.93, 115.94, 121.61, 122.35, 127.76, 129.18, 130.07, 132.04, 137.55, 138.06, 144.53, 155.68, 157.69, 159.84, 161.90 (C═O); Anal. Calcd for $C_{26}H_{23}N_3O_3$ (425.49): C, 73.39; H, 5.45; N, 9.88. Found: C, 73.23; H, 5.67; N, 10.09.

4.1.3.7. 3-(4-Chlorophenyl)-5-(4-methoxyphenyl)-1,4,5,7-tetrahydro-6H-[1,2]diazepino[4,3-c]quinolin-6-one (15 g). Off-white crystals, 82 % yield; m.p.: 295–297 °C; IR (υ_{max}, cm^{-1}): 3426 & 3298 (2NH), 3098 (CH-Ar.), 2970 (CH aliph.), 1647 (C═O); ^{1}H NMR (DMSO-d_6, 400 MHz): δ 3.04 (d, J = 13.7 Hz, 1H, CH of diazepine), 3.60 (s, 4H, CH of diazepine + OCH_3), 5.10 (d, J = 4.4 Hz, 1H, CH of diazepine), 6.67 (d, J = 8.2 Hz, 2H, Ar-Hs), 7.00 (d, 2H, J = 8.2 Hz, Ar-Hs), 7.20 (t, J = 7.5 Hz, 1H, Ar-H), 7.25–7.31 (m, 3H, Ar-Hs), 7.38 (d, J = 8.3 Hz, 2H, Ar-Hs), 7.49 (t, J = 7.5 Hz, 1H, Ar-H), 8.31 (d, J = 8.2 Hz, 1H, Ar-H), 10.35 (s, 1H, NH exchanged with D_2O), 11.30 (s, 1H, NH exchanged with D_2O); ^{13}C NMR (DMSO-d_6, 100 MHz): δ 38.08 (diazepine CH), 41.84 (diazepine CH_2), 55.39 (OCH_3), 110.65, 113.62, 113.84, 115.98, 121.69, 122.37, 128.00, 128.34, 129.08, 130.19, 133.36, 137.36, 138.06, 138.46, 144.31, 154.03, 157.78, 161.84 (C═O); Anal. Calcd for $C_{25}H_{20}ClN_3O_2$ (429.90): C, 69.85; H, 4.69; N, 9.77. Found: C, 69.73; H, 4.87; N, 10.01.

4.1.3.8. 3-(4-Bromophenyl)-5-(4-methoxyphenyl)-1,4,5,7-tetrahydro-6H-[1,2]diazepino[4,3-c]quinolin-6-one (15 h). Off-white crystals, 74 % yield; m.p.: 303–305 °C; IR (υ_{max}, cm^{-1}): 3433 & 3302 (2NH), 3098 (CH-Ar.), 2955 (CH aliph.), 1651 (C═O); ^{1}H NMR (DMSO-d_6, 400 MHz): δ 3.03 (d, J = 13.4 Hz, 1H, CH of diazepine), 3.60 (s, 4H, CH of diazepine + OCH_3), 5.10 (d, J = 4.8 Hz, 1H, CH of diazepine), 6.66 (d, J = 8.5 Hz, 2H, Ar-Hs), 7.00 (d, J = 8.5 Hz, 2H, Ar-Hs), 7.20 (t, J = 7.6 Hz, 1H, Ar-H), 7.31 (d, J = 8.5 Hz, 3H, Ar-Hs), 7.40 (d, J = 8.5 Hz, 2H, Ar-Hs), 7.49 (t, J = 7.6 Hz, 1H, Ar-H), 8.31 (d, J = 8.3 Hz, 1H, Ar-H), 10.36 (s, 1H, NH exchanged with D_2O), 11.31 (s, 1H, NH exchanged with D_2O); ^{13}C NMR (DMSO-d_6, 100 MHz): δ 38.04 (diazepine CH), 41.84 (diazepine CH_2), 55.38 (OCH_3), 110.70, 113.63, 113.84, 115.99, 121.70, 122.11, 122.37, 128.29, 129.08, 130.19, 131.26, 137.34, 138.07, 138.84, 144.31, 154.02, 157.78, 161.84 (C═O); MS *m/z* (%): 474.75 (M^+, 44.80), 476.17 (M^{+2}, 27.12), 400.08 (100); Anal. Calcd for $C_{25}H_{20}BrN_3O_2$ (474.36): C, 63.30; H, 4.25; N, 8.86. Found: C, 63.47; H, 4.32; N, 8.95.

X-Ray crystal structure determination. Crystallographic data for compound **15c** has been deposited with the Cambridge Crystallographic Data Center (CCDC) under the number 2301710. Copies of the data can be obtained, free of charge, by application to CCDC 12 Union Road, Cambridge CB2 1EZ, UK [Fax: +44–1223-336033; deposit@ccdc.cam.ac.uk http://www.ccdc.cam.ac.uk].

Single crystals of $C_{24}H_{18}ClN_3O$ (**15c**) are grown from EtOH/DMF (9:1, v:v). A suitable crystal was selected and mounted on a STOE IPDS 2 T diffractometer. The crystal was kept at 170 K during data collection. Using Olex2 [63], the structure was solved with the SHELXT [64] structure solution program using Intrinsic Phasing and refined with the SHELXL [65] refinement package using Least Squares minimization.

Crystal Data for $C_{24}H_{18}ClN_3O$ (**15c**) (M = 399.86 g/mol): monoclinic, space group $P2_1/n$ (no. 14), a = 13.3163(4) Å, b = 5.8032(2) Å, c = 25.1098(8) Å, β = 104.391(2)°, V = 1879.53(11) Å^3, Z = 4, T = 170 K, μ(Mo Kα) = 0.225 mm^{-1}, *Dcalc* = 1.413 g/cm^3, 18,223 reflections measured (5.228° ≤ 2Θ ≤ 58.406°), 5014 unique (R_{int} = 0.0671, R_{sigma} = 0.0404) which were used in all calculations. The final R_1 was 0.0489 (I > 2σ(I)) and wR_2 was 0.1318 (all data).

4.2. Biological assays

4.2.1. Inhibition assay of GSK-3β

ATP-Glo™ Kinase (BPS Bioscience, USA) assay was used in this investigation to evaluate GSK-3β activity [51]. A solution of 1 μM of the tested compound (prepared as 1 mM solution with DMSO and then diluted to the appropriate concentration), 2 μL GSK-3β kinase (0.6 ng/μl) and 2 μL of ATP (500 μM) /substrate (1 mg/ml) mixture was well mixed and added to each well. After incubation for 1 hr at 25 °C, 40 μL of termination-Glo reagent was added to cease the enzyme response and then remove the leftover ATP for 40 min. Then, the conversion of ADP to ATP took place for 30 min using 10 μL of kinase detection reagent. Finally, a multipurpose microplate reader (BioTek, USA) was used to record the luminous value. The drug's activity was proportionate to the difference between consumed and total ATP whereas inhibitory activities were estimated by comparing ATP levels in the presence and absence of inhibitor. Eight concentrations were used for each compound (100, 30, 10, 3, 1, 0.3, 0.1, and 0.03 nM), and three parallel runs of each

experiment were conducted. The IC_{50} values were calculated using GraphPad Prism 8.0 in accordance with the inhibitory activity of the tested compound at different dilutions.

4.2.2. Protein tau phosphorylation inhibition

The HTRF tau aggregation assay method [52,53] was used to quantify the amounts of tau aggregates in okadaic acid (OA) treated neuronal HT22 cells. HT22 cells were seeded at a density of 2×10^5 per well in 6-well plates. Following a 24-hour treatment period with compound **7c** and okadaic acid (**OA**), HT22 cells were gathered, subjected to a PBS wash, and then solubilized in ice-cold lysis buffer. The cell lysates underwent a 30-minute, 12,000 × g centrifugation at 4 °C. 10 μM of each sample was added to a 96-well black plate, then, a mixture of 5 μL of anti-tau-Tb^{3+} cryptate conjugate and 5 μL of anti-tau d2 conjugate were added to each well. The HTRF signals were monitored using multi-mode microplate reader after an overnight incubation at room temperature. Using the ratios of the two emission signals (665 and 620 nm), Delta F% (the levels of aggregated tau) was computed using the manufacturer's algorithm.

4.2.3. Cytotoxicity assays

MTT assay [54] was used to assess the cytotoxicity of test compound **7c** on hepatoma cells (THLE2) and human neuroblastoma cells (SH-SY5Y). Bronchial Epithelial Basal Medium (BEBM) was used to cultivate THLE-2 cells supplemented with 1 % fetal calf serum (FCS) and antibiotics (50 mg/ml penicillin, streptomycin, and gentamicin). SH-SY5Y cells were cultured in 5 % CO_2 at 37 °C in Eagle's minimum essential medium (EMEM) with 4.5 g/L glucose, 10 % fetal bovine serum FBS, 100U/mL penicillin, and 100 g/mL streptomycin. Replace the old medium by fresh medium with varying concentrations of the test compound (from 0.01 to 100 μM) and incubated for 24 h in a 37 °C humidified incubator. Following the incubation period, 20 μL of MTT was applied for 4 h, then the cultures were removed from the incubator and the resultant formazan crystals were dissolved with 200 μL of DMSO. At a wavelength of 490 nm, the absorbance was measured using a multifunctional microplate reader.

4.2.4. Kinetic studies

The overall procedure was identical to that for GSK-3β inhibition assay technique [51]. The kinetic studies were carried out to examine **7c**'s inhibitory mechanism on GSK-3β. Lineweaver-Burk reciprocal plots were performed using varying concentrations of inhibitor (0.1, 1.00, and 10 μM) and substrate (from 31.25 nM to 1000 nM), whereas ATP concentration remained unchanged (500 μM), in addition to a parallel experiment conducted without an inhibitor. Then, 1/velocity was plotted against 1/[Substrate] to construct lineweaver-Burk reciprocal plot. Data analysis was performed with Microsoft Excel 2016. The intersection of the curves served as a judge for the inhibitor interaction mechanism.

4.2.5. Selectivity profiling

At the International Centre for Kinase Profiling Division, University of Dundee (United Kingdom), compound **7c** was tested for kinase selectivity on a panel of 9 GSK-3β off-target kinases, from various families. In the presence of 10 μM of compound **7c**, protein kinase was tested. The selectivity profiling methodology has been provided in the supplementary file. (Supplementary S5.6.1).

4.2.6. In vivo behavioral studies

Healthy adult mice weighting 25–30 g were used in the present study. Animals were acclimatized in well-ventilated cages for one week at a temperature (25 ± 2 °C), humidity (60 ± 10 %), and lighting (12 h light–dark cycle). Food and water were available ad libitum. All the experimental procedures were performed according to approved protocols from the Research Ethics Committee for experimental and clinical studies at Faculty of Pharmacy, Cairo University (Approval number: PC 3429). After one-week adaptation, the mice were placed into four groups of five mice each: **i)** control (normal saline) group, **ii)** model (scopolamine) group (3 mg/kg, i.p.), **iii)** scopolamine plus donepezil (1 mg/kg, p.o.), **iv)** scopolamine plus compound **7c** (1 mg/kg, p.o.). For seven days, donepezil and test compounds were given orally to each group of animals once daily. On the seventh day, memory impairment induction by scopolamine was performed 30 min after donepezil or test compounds administration.

The passive avoidance test [57] was conducted in a device that had two different compartments separated by a sliding door. A dark compartment with an electrifiable grid floor was connected to the illuminated chamber, which was free of electric impulses. Each mouse was initially placed in the illuminated chamber so that it could become accustomed to it. The sliding door is then opened, allowing access to the dark gloomy compartment. The door was shut as soon as the animal entered the dark chamber entirely, and it was then shocked with an electric shock for two seconds (24 V, 0.5 mA). The transfer latency time (TLT) to enter the dark container was measured to assess the working memory (Training trial). A test experiment without the use of the electric foot shock was conducted twenty-four hours after the training trial.

4.3. Molecular Modeling Study

4.3.1. Molecular docking

The Molecular Operating Environment (MOE, 2022.02) software was used to achieve all the molecular docking studies. All minimizations were carried out with MOE until an RMSD gradient of 0.05 $kcal \bullet mol^{-1}Å^{-2}$ with Amber10:EHT force field and the partial charges were automatically calculated. GSK-3β protein crystal structure in conjunction with indirubin-3′-monoxime (IC_{50} = 22 nM) was obtained from the Protein Data Bank (PDB ID: 1Q41) [58] (https://www.rcsb.org).

Chain B and its co-crystalized water molecules were first removed, Then, the protein was prepared for the docking study using *QuickPrep* protocol in MOE with default options. The co-crystalized ligand was used to define the binding site for docking. Triangle Matcher placement method and London dG scoring function were used for docking. Self-docking of the co-crystallized ligand in the active site of the kinase domain was first performed to validate the used docking setup giving a docking pose with an energy score (S) = −12.02 kcal/mol and an RMSD of 0.262 Å.

The validated docking protocol was then used to study the ligand–protein interactions of compounds **7c**, **7e**, and **7f** in the kinase domain of GSK-3β to predict their binding mode and to rationalize their promising binding affinity.

4.3.2. Computational prediction of the ADME properties

The pharmacokinetic information relevant to our target derivatives was obtained using the free online swissADME [59,60] server (https://www.swissadme.ch/index.php). The physicochemical characteristics, pharmacokinetic features, and ADME parameters were all predicted and briefly explained.

4.3.3. Permeation of blood brain barrier (BBB)

BBB permeability of compounds was estimated using the CBLigand-BBB prediction server [61] and pkCSM [62].

4.3.4. Statistical analysis

All the statistical analytical studies were carried out using GraphPad Prism 9.5.0. software. GSK-3β inhibition assay results were analyzed using One Way ANOVA followed by Bonferroni Post hoc test while *in vivo* behavioral studies data were analyzed using student's *t* test.

CRediT authorship contribution statement

Esraa Abdo Moustafa: Writing – original draft, Methodology. **Heba Abdelrasheed Allam:** Writing – review & editing, Supervision. **Marwa A. Fouad:** Writing – review & editing. **Ahmed M. El Kerdawy:** Conceptualization, Writing – review & editing. **Nahed Nasser Eid El-Sayed:** Supervision, Data curation. **Christoph Wagner:** Methodology. **Hatem A. Abdel-Aziz:** Methodology. **Manal Abdel Fattah Ezzat:** Writing – original draft, Supervision, Methodology.

Declaration of competing interest

The authors declare that they have no known competing financial interests or personal relationships that could have appeared to influence the work reported in this paper.

Appendix A. Supplementary data

Supplementary data to this article can be found online at https://doi.org/10.1016/j.bioorg.2024.107324.

References

[1] K. Kumar, A. Kumar, R.M. Keegan, R. Deshmukh, Recent advances in the neurobiology and neuropharmacology of Alzheimer's disease, Biomed. Pharmacother. 98 (2018) 297–307.

[2] A. Wimo, L. Jonsson, J. Bond, M. Prince, B. Winblad, The worldwide economic impact of dementia 2010, Alzheimer's Dement. 9 (2013) 1–11.

[3] M.A. Ezzat, S.M. Abdelhamid, M.A. Fouad, H.A. Abdel-Aziz, H.A. Allam, Design, synthesis, in vitro, and in vivo evaluation of novel phthalazinone-based derivatives as promising acetylcholinesterase inhibitors for treatment of Alzheimer's disease, Drug Dev. Res. 84 (2023) 1231–1246.

[4] W. Liu, X. Jiang, Y. Zu, Y. Yang, Y. Liu, X. Sun, Z. Xu, H. Ding, Q. Zhao, A comprehensive description of GluN2B-selective N-methyl-D-aspartate (NMDA) receptor antagonists, Eur. J. Med. Chem. 15 (2020) 112447.

[5] S. Salomone, F. Caraci, G.M. Leggio, J. Fedotova, F. Drago, New pharmacological strategies for treatment of Alzheimer's disease: focus on disease modifying drugs, Br. J. Clin. Pharmacol. 73 (2012) 504–517.

[6] J.E. Gerson, D.L. Castillo-Carranza, U. Sengupta, M. Guerrero-Munoz, T. Masel, R. Kayed, P1–168: TAU oligomers as a mediator of toxicity in mixed protein pathology diseases, Alzheimer's Dement. 12 (2016) 467.

[7] M. Saitoh, J. Kunitomo, E. Kimura, H. Iwashita, Y. Uno, T. Onishi, N. Uchiyama, T. Kawamoto, T. Tanaka, C.D. Mol, D.R. Dougan, G.P. Textor, G.P. Snell, M. Takizawa, F. Itoh, M. Kori, 2-{3-[4-(alkylsulfinyl)phenyl]-1-benzofuran-5- yl}-5-methyl-1,3,4-oxadiazole derivatives as novel inhibitors of glycogen synthase kinase-3 beta with good brain permeability, J. Med. Chem. 52 (2009) 6270–6286.

[8] E.E. Congdon, E.M. Sigurdsson, Tau-targeting therapies for Alzheimer disease, Nat. Rev. Neurol. 14 (2018) 399–415.

[9] C.E. Tabit, S.M. Shenouda, M. Holbrook, J.L. Fetterman, S. Kiani, A.A. Frame, M. A. Kluge, A. Held, M.M. Dohadwala, N. Gokce, Protein kinase C-β contributes to impaired endothelial insulin signaling in humans with diabetes mellitus, Circulation 127 (2013) 86–95.

[10] X.L. Shi, J.D. Wu, P. Liu, Z.P. Liu, Synthesis and evaluation of novel GSK-3beta inhibitors as multifunctional agents against Alzheimer's disease, Eur. J. Med. Chem. 167 (2019) 211–225.

[11] M. Maqbool, M. Mobashir, N. Hoda, Pivotal role of glycogen synthase kinase-3β: a therapeutic target for Alzheimer's disease, Eur. J. Med. Chem. 107 (2016) 63–81.

[12] Y. Dong, J. Lu, S. Zhang, L. Chen, J. Wen, F. Wang, Y. Mao, L. Li, J. Zhang, S. Liao, L. Dong, Design, synthesis and bio-evaluation of 1,2,4-thiadiazolidine-3,5-dione derivatives as potential GSK-3β inhibitors for the treatment of Alzheimer's disease, Bioorg. Chem. 134 (2023) 10446.

[13] A.P. Paite, GSK-3β: a central kinase for neurodegenerative diseases? Med. Sci. 26 (2010) 516–521.

[14] H. Kittler, P. Tschand, Driver mutations in the mitogen-activated protein kinase pathway: the seeds of good and evil, Br. J. Dermat. 178 (2018) 26–27.

[15] O. Hantschel, Unexpected off-targets and paradoxical pathway activation by kinase inhibitors, ACS Chem. Biol. 10 (2015) 234–245.

[16] A. Lin, C.J. Giuliano, A. Palladino, K.M. John, C. Abramowicz, M.L. Yuan, E. L. Sausville, D.A. Lukow, L. Liu, A.R. Chait, Z.C. Galluzzo, C. Tucker, J.M. Sheltzer, Off-target toxicity is a common mechanism of action of cancer drugs undergoing clinical trials, Sci. Transl. Med. 11 (2019) eaaw8412.

[17] D. Bajusz, G.G. Ferenczy, G.M. Keseru, Structure-based virtual screening approaches in kinase-directed drug discovery, Curr. Top. Med. Chem. 17 (2017) 2235–2259.

[18] V. Lamba, I. Ghosh, New directions in targeting protein kinases: focusing upon true allosteric and bivalent inhibitors, Curr. Pharm. Des. 18 (2012) 2936–2945.

[19] S.M.A. Ruiz, H. Eldar-Finkelman, Glycogen synthase Kinase-3 inhibitors: preclinical and clinical focus on CNS-A decade Onward, Front. Mol. Neurosci. 14 (2021) 792364.

[20] C. Gao, Y.-L. Fan, F. Zhao, Q.-C. Ren, X. Wu, L. Chang, F. Gao, Quinolone derivatives and their activities against methicillin-resistant Staphylococcus aureus (MRSA), Eur. J. Med. Chem. 157 (2018) 1081–1095.

[21] X.-M. Chu, C. Wang, W. Liu, L.-L. Liang, K.-K. Gong, C.-Y. Zhao, K.-L. Sun, Quinoline and quinolone dimers and their biological activities: an overview, Eur. J. Med. Chem. 161 (2019) 101–117.

[22] X. Yang, P. Cai, Q. Liu, J. Wu, Y. Yin, X. Wang, L. Kong, Novel 8-hydroxyquinoline derivatives targeting β-amyloid aggregation, metal chelation and oxidative stress against Alzheimer's disease, Bioorg. Med. Chem. 12 (2018) 3191–3201.

[23] N.G. Faux, C.W. Ritchie, A. Gunn, A. Rembach, A. Tsatsanis, J. Bedo, J. Harrison, L. Lannfelt, K. Blennow, H. Zetterberg, M. Ingelsson, C.L. Masters, R.E. Tanzi, J. L. Cummings, C.M. Herd, A.I. Bush, PBT2 rapidly improves cognition in Alzheimer's disease: additional phase II analyses, J. Alzheimer's Dis. 20 (2010) 509–516.

[24] M. Pudlo, V. Luzet, L. Ismaïli, I. Tomassoli, A. Iutzeler, B. Refouvelet, Quinolone–benzylpiperidine derivatives as novel acetylcholinesterase inhibitor and antioxidant hybrids for Alzheimer disease, Bioorg. Med. Chem. 8 (2014) 2496–2507.

[25] B. Selvaraj, D.W. Kim, J.-S. Park, H.C. Kwon, H. Lee, K.-Y. Yoo, J.W. Lee, Neuroprotective effects of 2-heptyl-3-hydroxy-4-quinolone in HT22 mouse hippocampal neuronal cells, Bioorg. Med. Chem. Lett. 49 (2021) 128312.

[26] T. Shiro, T. Fukaya, M. Tobe, The chemistry and biological activity of heterocycle-fused quinolinone derivatives: a review, Eur. J. Med. Chem. 97 (2015) 397–408.

[27] W.P. Hong, I. Shin, H.N. Lim, Recent advances in one-pot Modular synthesis of 2-quinolones, Molecules 25 (2020) 5450.

[28] A.M. El Kerdawy, A.A. Osman, M.A. Zaater, Receptor-based pharmacophore modeling, virtual screening, and molecular docking studies for the discovery of novel GSK-3β inhibitor, J. Mol. Model. 25 (2019) 171.

[29] E. Damiens, B. Baratte, D. Marie, G. Eisenbrand, L. Meijer, Anti-mitotic properties of indirubin-3'-monoxime, a CDK/GSK-3 inhibitor: induction of endoreplication following prophase arrest, Oncogene 20 (2001) 3786–3797.

[30] P. Polychronopoulos, P. Magiatis, A.L. Skaltsounis, V. Myrianthopoulos, E. Mikros, A. Tarricone, A. Musacchio, S.M. Roe, L. Pearl, M. Leost, P. Greengard, L. Meijer, Structural basis for the synthesis of indirubins as potent and selective inhibitors of glycogen synthase kinase-3 and cyclin-dependent kinases, J. Med. Chem. 47 (2004) 935–946.

[31] P. Zhao, Y. Li, G. Gao, S. Wang, Y. Yan, X. Zhan, Z. Liu, Z. Mao, S. Chen, L. Wang, Design, synthesis and biological evaluation of N-alkyl or aryl substituted isoindigo derivatives as potential dual cyclin-dependent kinase 2 (CDK2)/glycogen synthase kinase 3β (GSK-3β) phosphorylation inhibitors, Eur. J. Med. Chem. 86 (2014) 165–174.

[32] W.M. Eldehna, S.T. Al-Rashood, T. Al-Warhi, R.O. Eskandrani, A. Alharbi, A.M. El Kerdawy, Novel oxindole/benzofuran hybrids as potential dual CDK2/GSK-3β inhibitors targeting breast cancer: design, synthesis, biological evaluation, and in silico studies, Journal of Enzyme Inhibition and Medicinal Chemistry 36 (2021) 270–285.

[33] S. Leclerc, M. Garnier, R. Hoessel, D. Marko, J.A. Bibb, G.L. Snyder, P. Greengard, J. Biernat, Y.Z. Wu, E.M. Mandelkow, G. Eisenbrand, L. Meijer, Indirubins inhibit glycogen synthase kinase-3 beta and CDK5/p25, two protein kinases involved in abnormal tau phosphorylation in Alzheimer's disease. a property common to most cyclin dependent kinase inhibitors? J. Biol. Chem. 376 (276) (2001) 251–260.

[34] M. Arfeen, S. Bhagat, R. Patel, S. Prasad, I. Roy, A.K. Chakraborti, P.V. Bharatam, Design, synthesis and biological evaluation of 5-benzylidene-2- iminothiazolidin-4-ones as selective GSK-3β inhibitors, Eur. J. Med. Chem. 121 (2016) 727–736.

[35] D. Tsvelikhovsky, S.L. Buchwald, Synthesis of heterocycles via pd-ligand controlled cyclization of 2-chloro-N-(2-vinyl)aniline: preparation of carbazoles, indoles, dibenzazepines, and acridines, J. Am. Chem. Soc. 132 (2010) 14048.

[36] A.K. Ramasamy, V. Balasubramaniam, K. Mohan, Synthesis and Characterization of substituted 4-methoxy-1H-quinolin-2-ones, E-J. Chem. 7 (2010) 1066–1070.

[37] R.J. Rowlett Jr, R.E. Lutiz, Antimalarials; hydrolysis and methanolysis of 2,4,7-trichloroquinoline, J. Am. Chem. Soc. 68 (1946) 1288–1291, https://doi.org/10.1021/ja01211a050.

[38] E. Hayashi, N. Shimada, The reaction of heteroaromatic N-oxide with acid chloride and cyanide. III. on the reaction of quinoline N-oxides with sulfonic acid chloride and potassium cyanide, J. Pharm. Soc. Jpn. 97 (1977) 627–640, https://doi.org/10.1248/yakushi1947.97.6_627.

[39] M.M. Ismail, M. Abbas, M.M. Hassan, Chemistry of substituted quinolinones. Part VI. synthesis and nucleophilic reactions of 4-Chloro-8-methylquinolin-2(1H)-one and its thione analogue, Molecules 5 (2000) 1224–1239.

[40] C.H. Nguyen, C. Marchand, S. Delage, J.S. Sun, T. Garestier, C. Hélène, E. Bisagni, Synthesis of 13 H-benzo [6, 7]-and 13 H-benzo [4, 5] indolo [3, 2-c]-quinolines: a new series of potent specific ligands for triplex DNA, J. Am. Chem. Soc. 120 (1998) 2501–2507, https://doi.org/10.1021/ja971707x.

[41] R.A. Howie, M.V.N. de Souza, M. Ferreira de Lima, C.R. Kaiser, J.L. Wardell, S.M.S. V. Wardell, Structures of arylaldehyde 7-chloroquinoline-4-hydrazones: supramolecular arrangements derived from N—H……N, C—H__X(X = N, O, or Π) and Π__Π interactions Z. Kristallogr. 225 (2010) 440–447. https://doi.org/10.1524/zkri.2010.1291.

[42] S. Eswaran, A.V. Adhikari, I.H. Chowdhury, N.K. Pal, K.D. Thomas, New quinoline derivatives: synthesis and investigation of antibacterial and antituberculosis properties, Eur. J. Med. Chem. 45 (2010) 3374–3383, https://doi.org/10.1016/j.ejmech.2010.04.022.

[43] M.A.I. Elbastawesy, M. Ramadan, Y.A.M.M. El-Shaier, A.A. Aly, G.E.A. Abuo-Rahma, Arylidenes of Quinolin-2-one scaffold as erlotinib analogues with activities against leukemia through inhibition of EGFR TK/ STAT-3 pathways, Bioorg. Chem. 96 (2020) 103628, https://doi.org/10.1016/j.bioorg.2020.103628.

[44] T.D. Le, N.N. Pham, T.C. Nguyen, Preparation and antibacterial activity of some new 4-(2-heterylidenehydrazinyl)-7-chloroquinoline derivatives, J. Chem. 2018 (2018) 1–7, https://doi.org/10.1155/2018/4301847.
[45] V.M. Dziomko, M.N. Stopnikova, L.V. Shmelev, Y.S. Ryabokobylko, G. M. Adamova, R.V. Poponova, Structure and isomerism of 2-(3-substituted) quinoxalinyl-hydrazones of isatin and its homologs, Chemistry of Heterocyclic Compounds 16 (1980) 1073–1078.
[46] Ö.S. Eter, Z. Atioğlu, M. Akkurt, C.C. ERSANLI, N. KARALI, Molecular and crystal structure of 1-methyl-5-trifluoromethoxy-1H-indole-2, 3-dione 3-[4-(4-methoxy-phenyl) thiosemicarbazone], İstanbul J. Pharm., 51 (2021) 59-66.
[47] R. Šandrik, P. Tisovský, K. Csicsai, J. Donovalová, M. Gáplovský, R. Sokolík, J. Filo, A. Gáplovský, ON/OFF photostimulation of isatin bipyridyl hydrazones: photochemical and spectral study, Molecules 24 (2019) 2668, https://doi.org/10.3390/molecules24142668.
[48] M. Cigáň, K. Jakusová, M. Gáplovský, J. Filo, J. Donovalová, A. Gáplovský, Isatin phenylhydrazones: anion enhanced photochromic behaviour, Photochem. Photobiol. Sci. 14 (2015) 2064–2073, https://doi.org/10.1039/C5PP00275C.
[49] S.M. Mostafa, A.A. Aly, A.A. Hassan, E.M. Osman, S. Bräse, M. Nieger, M.A. A. Ibrahim, A.H. Mohamed, Autoxidation of 4-Hydrazinylquinolin-2(1H)-one; synthesis of Pyridazino[4,3-c:5,6-c']diquinoline-6,7(5H,8H)-diones, Molecules 27 (2022) 2125.
[50] F. Kenari, S. Molnár, P. Perjési, Reaction of chalcones with Cellular thiols. the effect of the 4-substitution of chalcones and protonation state of the thiols on the addition process. diastereoselective thiol addition, Molecules 26 (2021) 4332.
[51] W. Liu, X. Liu, W. Liu, Y. Gao, L. Wu, Y. Huang, H. Chen, D. Li, L. Zhou, N. Wang, Z. Xu, X. Jiang, Q. Zhao, Discovery of novel beta-carboline derivatives as selective AChE inhibitors with GSK-3beta inhibitory property for the treatment of Alzheimer's disease, Eur. J. Med. Chem. 229 (2022) 114095.
[52] X. Liu, W. She, H.-H.-Y. Sung, I.D. Williams, P. Qian, Tau-aggregation inhibitors derived from Streptomyces tendae MCCC 1A01534 protect HT22 cells against okadaic acid-induced damage, Int. J. Biol. Macromol. 231 (2023) 123170.
[53] Z. Zhang, J.W. Simpkins, An okadaic acid-induced model of tauopathy and cognitive deficiency, Brain Res. 1359 (2010) 233–246, https://doi.org/10.1016/j.brainres.2010.08.077.
[54] X. Li, H. Wang, Z. Lu, X. Zheng, W. Ni, J. Zhu, Y. Fu, F. Lian, N. Zhang, J. Li, H. Zhang, F. Mao, Development of multifunctional pyrimidinylthiourea derivatives as potential anti-Alzheimer agents, J. Med. Chem. 59 (2016) 8326–8344, https://doi.org/10.1021/acs.jmedchem.6b00636.
[55] P. Jain, C. Karthikeyan, N.S. Hari, N. Moorthy, D.K. Waiker, A.K. Jain, P. Trivedi, Human CDC2-like kinase 1 (CLK1): a novel target for Alzheimer's disease, Curr. Drug Targets 5 (2014) 539–550.
[56] C. Albertini, A. Salerno, P. de Sena Murteira, M.L.B. Pinheiro, From combinations to multitarget-directed ligands: a continuum in Alzheimer's disease polypharmacology, Med. Res. Rev. 41 (2021) 2606–2633.
[57] Z. Bohdanecký, M. Jarvik, Impairment of one-trial passive avoidance learning in mice by scopolamine, scopolamine methylbromide, and physostigmine, Int. J. Neuropharmacol. 6 (1967) 217–222, https://doi.org/10.1016/S0163-1047(88)90938-7.
[58] J.A. Bertrand, S. Thieffine, A. Vulpetti, C. Cristiani, B. Valsasina, S. Knapp, H. M. Kalisz, M. Flocco, Structural Characterization of the GSK-3β active site using selective and non-selective ATP-mimetic inhibitors, J. Mol. Biol. 333 (2003) 393–407, https://doi.org/10.1016/j.jmb.2003.08.031.
[59] A. Daina, O. Michielin, V. Zoete, SwissADME: A free web tool to evaluate pharmacokinetics, drug-likeness and medicinal chemistry friendliness of small molecules, Sci. Rep. 7 (2017) 42717, https://doi.org/10.1038/srep42717.
[60] D. Li, W. Liu, Y. Huang, M. Liu, C. Tian, H. Lu, H. Jia, Z. Xu, H. Ding, Q. Zhao, Facile synthesis of C1-substituted beta-carbolines as CDK4 inhibitors for the treatment of cancer, Bioorg. Chem. 121 (2022) 105659.
[61] X.-Q.S.X.s. laboratory, The blood-brain barrier (BBB) Prediction Server, May 2010. https://www.cbligand.org/BBB/index.php. (Accessed 14/12 2023).
[62] D.E. Pires, T.L. Blundell, D.B. Ascher, pkCSM: predicting small-molecule pharmacokinetic and toxicity properties using graph-based signatures, J. Med. Chem. 58 (9) (2015) 4066–4072.
[63] O.V. Dolomanov, L.J. Bourhis, R.J. Gildea, J.A.K. Howard, H. Puschmann, J. Appl. Cryst. 42 (42) (2009) 339–341.
[64] G.M. Sheldrick, SHELXT-integrated space-group and crystal-structure determination. acta crystallographica section, acta cryst., a, A 71 (2015) 3–8.
[65] G.M. Sheldrick, Crystal structure refinement with SHELXL, acta crystallogr. C struct chem, C 71 (2015) 3–8.